Integral equation methods from grating theory to photonics: An overview and new approaches for conical diffraction

Bernd H. Kleemann

Journal of Modern Optics
Vol. 00, No. 00, 10 January 2008, 1–23

Research Article

Integral equation methods from grating theory to photonics: An overview and new approaches for conical diffraction

Gunther Schmidt[a] and Bernd H. Kleemann[b*]

[a] *Weierstrass – Institute for Applied Analysis and Stochastics, D-10117 Berlin, Germany*; [b] *Corporate Research and Technology, Carl Zeiss AG, D-73446 Oberkochen, Germany*

(*Received 8 June 2010; final version received 10 October 2010*)

The boundary integral equation method (BIM) was one of the first methods in grating theory. It has been used for the investigation of diffraction gratings of extremely different kind as well as for photonic crystal diffraction gratings. Besides an overview of three of the most important BIMs for in-plane diffraction, we present a new BIM for gratings in conical mounting with one profile as well as for separated multilayer gratings with photonics inclusions using a common description for both approaches. In numerical examples, (1) blazing in conical mounting is demonstrated at a photonic crystal diffraction grating, (2) the excellent conical efficiency convergence for a plasmonic structure of two stacked silver rod gratings is shown, and (3) the transmission for conical incidence is studied at a blazed grating with large period to wavelength ratio.

Keywords: integral equation method; conical diffraction; diffraction gratings; photonic crystal gratings; plasmonic multilayer gratings

1. Introduction

Considering electromagnetic methods for diffractive optics and photonics it is worth noting that the starting point for these methods were electromagnetic methods for gratings. Gratings exist already since about 1821 – and after a long time of scalar theories, since the 1970s, there emerged several different electromagnetic methods for the computation of the polarisation dependent complex diffraction amplitudes – for several types of gratings. Consequently, electromagnetic diffraction methods are established for some decades for spectroscopic gratings (*1–3*), 'moth eye'-anti reflective structures (*4*), non-paraxial beam splitters and gratings with polarisation dependent optical functions (*5*), for example. Comprehensive collections with detailed mathematical descriptions and physical interpretations of the state-of-the-art methods for gratings at that time are given in (*6, 7*).

In the 1980s and 1990s these methods became more and more popular and have been applied to a variety of diffraction problems also in diffractive optics. It has been shown that electromagnetic diffraction methods are useful for the analysis and improvement (i.e. optimisation) as well as for the synthesis of gratings (*8, 9*) which have been designed by scalar methods but have been applied in the region between paraxial and non-paraxial applicability. In the overview (*10*), several electromagnetic methods in diffractive optics are summarized and some of their applications are discussed.

Especially the local linear grating assumption (LLGA) introduced in (*11*) was a big step forward to the electromagnetic treatment of large diffractive lenses. Assuming a linear grating at local positions of curved lines of diffractive lenses made the application of electromagnetic grating methods possible. Fresnel-lenses, Bragg-Fresnel-lenses, cylindrical lens arrays, but also

*Corresponding author. Email: b.kleemann@zeiss.de

ISSN: 0950-0340 print/ISSN 1362-3044 online

DOI: 10.1080/0950034YYxxxxxxxx
http://www.informaworld.com

general (holographic as well as digital) beam- and wavefront shaping elements, summarized as Fresnel-zone plates (FZPs), nowadays have increasing applications in measurement and for the coupling of laser beams. At first, the LLGA was used in (*11*) for the description and optimisation of cylindrical lens arrays and in (*12, 13*) for the analysis and synthesis of micro Fresnel-lenses, including the calculation of the polarisation dependent point spread functions in the focus. Depending on the numerical aperture (NA) of the FZPs, they often possess minimal zone widths in the range of the wavelength. The prediction of scalar methods may be too inaccurate for an exact modelling and electromagnetic methods have to be used for zone widths smaller than about 10 wavelengths (*14*).

Surely, the LLGA is an approximation and its application introduces errors compared to a possibly exact modelling. However, this would imply the electromagnetic modelling of a complete FZP at once or at least of a cross section in case of a cylindrical FZP. The following methods apply to the last item. The far field intensity distribution in reflection has been calculated in (*15*) for an ideal conducting material (infinite conductivity model) of a cylindrical non-periodic diffractive structure using a boundary integral method. A coupled finite element method – boundary element method (FEM–BEM) has been introduced in (*16*) and some diffractive elements have been optimized in (*17*) using this method. Later, a boundary integral method has been implemented in (*18*), working for dielectric materials, too. The full NA is considered in (*19*) using a volume integral method for the optimisation of the phase distribution in the far field. All these methods are able to model cross sections of FZPs with a diameter of only some hundreds of wavelengths in maximum due to a necessary discretisation. Hence, FZPs or Fresnel-lenses with large diameters or cross sections compared to the wavelength cannot be treated using these fully electromagnetic methods. Since most FZPs have cross sections or diameters from thousands to millions of wavelengths this applies to most FZPs and Fresnel-lenses and particularly to kinoforms.

At that point, one-dimensional electromagnetic methods for grating diffraction come into play together with a plane wave decomposition of the incident field and the LLGA. Assuming a sufficiently large number of zones, a slowly varying zone width, and smoothly curved zones, LLGA allows for the calculation of complex diffraction amplitudes at local zone positions for each of the plane waves. A phase-correct superposition of all local amplitudes allows for the calculation of the point spread function or secondary quantities to qualifying an optical system (*12, 13, 20*), for example.

In the last ten years, the possibilities for fabrication of structures in the order and below the order of the wavelength expanded significantly (*21, 22*). Using photolithographic methods, for example, 32 nm – 90 nm 'wide' structures on the Si-wafer are really mastered, and smaller structures can be fabricated soon. Hence, electromagnetic methods become more and more important for the simulation of diffractive and photonic structures.

The boundary integral equation method (BIM) was one of the first methods in grating theory. It has been used for the investigation of diffraction gratings of extremely different kind including photonic crystal diffraction gratings. Our aim is to give an overview on three of the most important BIMs for in-plane diffraction highlighting the corresponding literature over some four decades in what is now a fully developed theory (cf. Sect. 3). Afterwards we present extensions of the integral method to solve the problem of conical (off-plane) diffraction in Sect. 4. In detail we report on recent results on conical diffraction of a finitely conducting interface in Sect. 4.1 and we present a new solution method for separated multilayer gratings with photonics inclusions using a common description for both approaches in Sects. 4.2 – 4.5. Examples applying the new methods in Sect. 5 conclude the work. Especially, (1) blazing in conical mounting is demonstrated at a photonic crystal diffraction grating generalising a result from the literature achieved for in-plane diffraction, (2) the excellent conical efficiency convergence for a plasmonic structure of two stacked silver rod gratings is shown, and (3) the transmission for conical incidence is studied at a blazed grating with large ratio of period to wavelength showing the ability of the new method. We start by defining the physical problem in the next section.

2. The Physical Problem for one profile

The grating surface $\Sigma \times \mathbb{R}$ is given by a d-periodic, non self-intersecting curve Σ in the (x, y)-plane. Depending on the particular method, there may be additional conditions necessary on Σ, for instance, it may not have edges if the numerical method does not allow it, or there is no overhanging profile allowed. We refer to these differences in the description of the particular method.

PLEASE INSERT FIGURE 1 ABOUT HERE

The surface $\Sigma \times \mathbb{R}$ separates two regions $G_\pm \times \mathbb{R} \subset \mathbb{R}^3$ filled with homogeneous and isotropic materials of arbitrary real or complex electric permittivity $\varepsilon_\pm$ and magnetic permeability $\mu_\pm$, see Figure 1. The (complex) refractive index of the material is given by $n_\pm = c_o(\varepsilon_\pm \mu_\pm)^{1/2}$, with c_o the speed of light and $c_o = (\varepsilon_{\text{vacuum}}\, \mu_{\text{vacuum}})^{-1/2}$.

It is assumed that the light in form of a monochromatic plane wave with wavelength λ and given polarisation is incident on the grating from $G_+ \times \mathbb{R}$, which is filled with a lossless material. We consider the general case of conical diffraction, i.e., we allow that the wave vector $\boldsymbol{k} = (\alpha, -\beta, \gamma)$ of the incident electric field

$$\boldsymbol{P} \exp\bigl(\mathrm{i}(\alpha x - \beta y + \gamma z)\bigr) = \boldsymbol{E}^{\text{in}} \exp(\mathrm{i}\gamma z)$$

is not in the $x0y$ plane. Then $\boldsymbol{k}$ can be expressed in terms of the incidence angles ϕ (the angle between $\boldsymbol{k}$ and its projection on the $x0y$ plane) and θ (the angle of that projection with the $0y$ axis):

$$\boldsymbol{k} = |\boldsymbol{k}|(\sin\theta\cos\phi, -\cos\theta\cos\phi, \sin\phi) \quad \text{with} \quad |\boldsymbol{k}| = \omega(\varepsilon_+\mu_+)^{1/2}\,,\ \omega = \frac{2\pi}{\lambda}\,. \tag{1}$$

The complex valued vector $\boldsymbol{P}$ is orthogonal to $\boldsymbol{k}$ and it is convenient to specify the polarisation by the angles

$$\delta^{\text{in}} = \arctan\frac{|(\boldsymbol{P}, \boldsymbol{s})|}{|(\boldsymbol{P}, \boldsymbol{p})|}\,, \quad \psi^{\text{in}} = -\arg\frac{(\boldsymbol{P}, \boldsymbol{s})}{(\boldsymbol{P}, \boldsymbol{p})}\,,$$

where the unit vector $\boldsymbol{s}$ is orthogonal to the incident plane spanned by $\boldsymbol{k}$ and the grating normal $(0, 1, 0)$ and $\boldsymbol{p} = (\boldsymbol{s} \times \boldsymbol{k})/|\boldsymbol{k}|$.

For the following, we introduce the function κ taking two constant values

$$\kappa(x, y) = \begin{cases} \kappa_+ = (\mu_+\varepsilon_+ - \varepsilon_+\mu_+ \sin^2\phi)^{1/2} & (x, y) \in G_+\,, \\ \kappa_- = (\mu_-\varepsilon_- - \varepsilon_+\mu_+ \sin^2\phi)^{1/2} & (x, y) \in G_-\,, \end{cases} \tag{2}$$

where we choose the square root $z^{1/2} = r^{1/2}\exp(\mathrm{i}\varphi/2)$ for $z = r\exp(\mathrm{i}\varphi)$, $0 \le \varphi < 2\pi$. Under the assumption $\kappa(x, y) \neq 0$ the time-harmonic electromagnetic formulation of conical diffraction can be transformed to a problem for two scalar functions in the $x0y$ plane. Writing the electromagnetic field vectors $\mathbf{E}$ and $\mathbf{H}$ in the form

$$\mathbf{E}(x, y, z) = \boldsymbol{E}(x, y)\exp(\mathrm{i}\gamma z)\,,\ \mathbf{H}(x, y, z) = \boldsymbol{H}(x, y)\exp(\mathrm{i}\gamma z)$$

and denoting $\boldsymbol{B} = (\mu_+/\varepsilon_+)^{1/2}\,\boldsymbol{H}$, the Maxwell system implies that the z-components $E_{\text{z}}, B_{\text{z}}$ of the vector functions $\boldsymbol{E}$ and $\boldsymbol{B}$ satisfy Helmholtz equations in $G_\pm$

$$(\Delta + \omega^2\kappa_\pm^2)\, E_{\text{z}} = (\Delta + \omega^2\kappa_\pm^2)\, B_{\text{z}} = 0\,, \tag{3}$$

and that they are coupled at the interface Σ by so-called transmission conditions

$$\left[E_{\mathrm{z}}\right]_{\Sigma} = \left[B_{\mathrm{z}}\right]_{\Sigma} = 0\,,\ \left[\frac{\varepsilon\,\partial_{\mathrm{n}}E_{\mathrm{z}}}{\kappa^2} + \varepsilon_+ \sin\phi\frac{\partial_{\mathrm{t}}B_{\mathrm{z}}}{\kappa^2}\right]_{\Sigma} = \left[\frac{\mu\,\partial_{\mathrm{n}}B_{\mathrm{z}}}{\kappa^2} - \mu_+ \sin\phi\frac{\partial_{\mathrm{t}}E_{\mathrm{z}}}{\kappa^2}\right]_{\Sigma} = 0\,, \tag{4}$$

where $\left[f\right]_{\Sigma}$ denotes the jump of a function f across the interface Σ, and ∂_{n} and ∂_{t} are the normal and tangential derivatives, respectively.

Furthermore, $E_{\mathrm{z}}, B_{\mathrm{z}}$ must be α quasiperiodic in x, i.e. $E_{\mathrm{z}}(x+d,y) = \exp(\mathrm{i}\alpha d)E_{\mathrm{z}}(x,y)$, and satisfy the outgoing wave condition, ensuring the finiteness of the scattered field:
If $H \in \mathbb{R}$ is chosen such that the grating structure is contained in $\{|y| < H\}$, i.e. $\kappa(x,y) = \kappa_+$ and $\kappa(x,-y) = \kappa_-$ for $y \geq H$, then the representations

$$\begin{aligned}(E_{\mathrm{z}}, B_{\mathrm{z}}) - (E_{\mathrm{z}}^{\mathrm{in}}, B_{\mathrm{z}}^{\mathrm{in}}) &= \sum_{n\in\mathbb{Z}} (E_n^+, B_n^+)\exp(\,\mathrm{i}(\alpha_n x + \beta_n^+ y)), \quad y \geq H,\\ (E_{\mathrm{z}}, B_{\mathrm{z}}) &= \sum_{n\in\mathbb{Z}} (E_n^-, B_n^-)\exp(\,\mathrm{i}(\alpha_n x - \beta_n^- y)), \quad y \leq -H,\end{aligned} \tag{5}$$

are valid with complex constants $E_n^{\pm}, B_n^{\pm}$, the unknown Rayleigh coefficients. Here we use the notation

$$\alpha_n = \alpha + \frac{2\pi\, n}{d}\,, \quad \beta_n^{\pm} = (\omega^2\kappa_{\pm}^2 - \alpha_n^2)^{1/2}\,,\ n \in \mathbb{Z}\,, \tag{6}$$

where the square root is defined as in relation (2) and $E_{\mathrm{z}}^{\mathrm{in}}\exp(\mathrm{i}\gamma z)$, $B_{\mathrm{z}}^{\mathrm{in}}\exp(\mathrm{i}\gamma z)$ are the z-components of the incoming plane wave. Since $\Im(\beta_n^{\pm}) \geq 0$, the sums in equations (5) remain bounded for $y \to \pm\infty$.

3. Integral methods for in-plane diffraction

By experts knowing various electromagnetic methods, boundary integral equation methods (short: integral methods) are often considered as the ideal electromagnetic method for the investigation of diffraction gratings (cf. e.g. (*3*, p. 370)). This surely comes from the high accuracy and good convergence of the methods in a wide range of diffraction problems. However, the mathematical complexity of the integral methods is high and several pitfalls exist during mathematical formulation and numerical implementation. Hence, for the integral methods, there will probably never be a publication with a description of the algorithm for the optical engineer as it exists for the C-method (*23*). But, if correctly implemented, integral methods belong to the most general and fastest methods available. We cite from (*3*, p. 383): 'As a result of its generality, the integral theory is able to deal with practically any kind of grating, including some limiting cases where it is the only available method.' Examples are especially echelle gratings used in high orders and at high angles of incidence (*24–27*).

Interestingly, in spite of its complexity, integral methods belong to the first electromagnetic methods investigated theoretically and numerically for grating diffraction calculations, starting in the mid 1960s. This was mainly due to the good convergence of the integral methods especially for transverse-magnetic (TM) polarisation.

Additionally, the integral formalism has a close physical connection and hence, can be explained in a very simple and intuitive manner, given in (*7*, p. 37). The most important and comprehensive summary on integral methods known until the 1980s is given in (*7, 28*), including the theoretical and numerical difficulties. Meanwhile, several new or improved integral methods have been published:

- using two integral equations instead of one for one profile including an efficient algorithm for overcoated gratings (*29–31*),
- for multilayer gratings with a large number of layers (*32, 33*),
- with faster and more stable kernel function evaluation (*34*),
- with better convergence properties for profiles with edges and for thin coatings (*34*).

However, all these methods treat only in-plane diffraction problems, where $\phi = 0$. Then $\kappa_j^2 = \varepsilon_j \mu_j$ and conditions (4) pass into the well known conditions on the jump through the interface

$$\big[E_{\mathrm{z}}\big]_\Sigma = \big[B_{\mathrm{z}}\big]_\Sigma = \big[\mu^{-1}\partial_{\mathrm{n}} E_{\mathrm{z}}\big]_\Sigma = \big[\varepsilon^{-1}\partial_{\mathrm{n}} B_{\mathrm{z}}\big]_\Sigma = 0\,. \tag{7}$$

Together with these jump conditions, the in-plane diffraction problem (3) – (5) splits into separate problems for TE (transverse-electric) and TM polarisation, respectively.

Only recently an integral method for real conical diffraction for a single grating has been published and implemented (*35, 36*) leading to an inherently coupled integral equation system. An outline of this method and an extension to multi-profile diffraction gratings is presented in Sect. 4.

3.1. *Potential-theoretic basis*

The integral formulation is based on the application of potential-theoretic methods to the underlying differential equations. Quasiperiodic solutions of the Helmholtz equation $(\Delta + \omega^2 \kappa_\pm^2) u = 0$ satisfying outgoing wave conditions of the form of equations (5) can be represented as potentials of the single layer $\mathcal{V}^\pm$ or of the double layer $\mathcal{K}^\pm$ defined by

$$\mathcal{V}^\pm \varphi(P) = \int_\Gamma \varphi(Q) \Psi_{\kappa_\pm,\alpha}(P-Q)\,\mathrm{d}\sigma(Q)\,, \quad \mathcal{K}^\pm \varphi(P) = \int_\Gamma \varphi(Q) \partial_{\mathrm{n}(Q)} \Psi_{\kappa_\pm,\alpha}(P-Q)\,\mathrm{d}\sigma(Q) \tag{8}$$

for $P \in G_\pm$. Here φ is an unknown density on Γ, which is one period of the profile curve Σ, and the integral kernel is the fundamental solution of quasiperiodic Helmholtz equations

$$\Psi_{\kappa_\pm,\alpha}(P) = \lim_{N\to\infty} \frac{\mathrm{i}}{d} \sum_{n=-N}^{N} \frac{\exp(\,\mathrm{i}\alpha_n X + \mathrm{i}\beta_n^\pm |Y|)}{\beta_n^\pm}\,, \quad P = (X,Y)\,, \tag{9}$$

where $\alpha_n, \beta_n^\pm$ are as in equation (6). It is assumed that $\beta_n^\pm \neq 0$ for all $n \in \mathbb{Z}$ and $j = 0, 1$. Otherwise, the terms of the fundamental solution with $\beta_n^\pm = 0$ can be replaced by $\exp(\,\mathrm{i}\alpha_n X)$, leading formally to the same equations, but some modifications in their analytical and numerical treatment are necessary. A more practical treatment of the degenerate case consists in using the original equations but by a small amount modified wavelengths, thus avoiding the singularity case.

Another representation of those solutions u is given by Green's formula

$$u = \frac{1}{2}\big(\mathcal{V}^+ \partial_{\mathrm{n}} u - \mathcal{K}^+ u\big) \quad \text{in } G_+\,, \quad u = \frac{1}{2}\big(\mathcal{K}^- u - \mathcal{V}^- \partial_{\mathrm{n}} u\big) \quad \text{in } G_-\,. \tag{10}$$

The integral equations for the unknown densities or boundary values on Γ are then obtained from the transmission conditions (4) and from the known jump relations for the layer potentials.

Due to the different integral representations, there have been developed different integral methods. Three of the most important methods are outlined in the following parts of this section highlighting some pros and cons. Whereas in (*28, 37*), the boundary value problem is transformed into a *single* integral equation (cf. Sect. 3.2), it is transformed into a special integral equation *system* in (*29–31*) presented in Sect. 3.4 including several improvements (*34*). Another method

(*38*) based on the first approach, which is able to treat multilayer gratings with a large number of layers (*32, 33*), is presented in Sect. 3.3.

We try to characterize the following integral methods by e.g.:

- theoretical formulation (one or two equations, first or second kind),
- numerical solution method (trigonometric, splines, collocation, others),
- kernel function evaluation,
- profile representation: functional or arc length,
- treating of edges.

3.2. *Single equation integral method*

One of the first stable integral methods for finite conductivity, often tried to copy, was the one, presented in (*37, 39, 40*) by D. Maystre. This author and his numerous creative publications have significantly influenced the development of electromagnetic methods and especially of integral methods for grating theory and photonics in a manifold manner. For a better distinction, let us name this method simply IEM (integral equation method). When the method was introduced, Σ should be given by a smooth function, hence overhangings, vertical side walls and profiles with edges were not allowed and the discretisation was carried out along the x-axis. As described in (*28*), it combines single layer potential representations

$$E_{\mathrm{z}} = \mathcal{V}^{-} w\,,\ B_{\mathrm{z}} = \mathcal{V}^{-} \tau\,, \tag{11}$$

in the bottom layer G_- (cf. Figure 1) and Green's formula applied to $E_{\mathrm{z}} - E_{\mathrm{z}}^{\mathrm{in}}$ and $B_{\mathrm{z}} - B_{\mathrm{z}}^{\mathrm{in}}$ in G_+. Then the transmission conditions (7) lead to single integral equations for the unknown densities

$$\begin{aligned} \Big(\frac{\mu_+}{\mu_-}\, V^+(I - L^-) + (I + K^+)V^-\Big) w &= -2E_{\mathrm{z}}^{\mathrm{in}}\,, \\ \Big(\frac{\varepsilon_+}{\varepsilon_-}\, V^+(I - L^-) + (I + K^+)V^-\Big) \tau &= -2B_{\mathrm{z}}^{\mathrm{in}}\,. \end{aligned} \tag{12}$$

Here and in the following we use the boundary integrals ($P \in \Gamma$)

$$\begin{aligned} V^{\pm}\varphi &= \int_\Gamma \varphi(Q)\, \Psi_{\kappa_\pm,\alpha}(P-Q)\, \mathrm{d}\sigma_Q\,,\ K^{\pm}\varphi = \int_\Gamma \varphi(Q)\, \partial_{\mathrm{n}(Q)} \Psi_{\kappa_\pm,\alpha}(P-Q)\, \mathrm{d}\sigma_Q\,, \\ L^{\pm}\varphi &= \int_\Gamma \varphi(Q)\, \partial_{\mathrm{n}(P)} \Psi_{\kappa_\pm,\alpha}(P-Q)\, \mathrm{d}\sigma_Q\,. \end{aligned} \tag{13}$$

The formulations (12) of a single equation for TE and TM polarisation, respectively, has been considered as advantage in (*3*) although several problems occur with the calculation of the double integrals, the solution of which has been addressed and solved in (*28, 37*). Also for highly conducting gratings the equations (12) work well: when $\Im(n_-) \to \infty$, then they tend towards the integral equations describing perfectly conducting gratings. Additionally, this formalism has been generalised to more complicated gratings of practical interest, for instance for metallic or dielectric gratings covered with a stack of dielectric layers (*28, 41–44*), or bimetallic gratings, i.e., gratings whose surface is composed of two alternating metals (*44, 45*).

Very interesting is the approach for multiprofile gratings presented in (*41*) as it allows for a consecutive solution for a large number of layers. For this reason it is used in the modified integral method (*46*) (cf. Sect. 3.3). In each step the solution is determined from the field of the step before starting with the uppermost layer, however, each step requires a matrix inversion of $\mathcal{O}(N^3)$ operations with N the dimension of the matrix.

Already in (*7*) one finds the first hint that the integral formalism 'applies as well, provided that s is used instead of x in the integrals', with s being the arc length of the profile function, depending on x and thus describing a profile parametrisation. This has been realised and demonstrated in (*47*), the first specific publication on the diffraction at coated echelles with 'conformal' layer. The implementation of the new integral method now includes also parametrised profile curves and refinement of quadrature nodes at edges, which makes it possible to treat echelle gratings with thin dielectric layers on a deep grating profile having edges and a large period. Also, profiles with overhangings and vertical side walls can now be treated. This method has been applied to an extensive investigation of echelle gratings (*24*) ranging from low (8 ... 13) to very high (up to 660) diffraction orders and a year later to extremely high orders (*25*).

Another approach for gratings with multiple profiles without interpenetration is proposed in (*42*). It is based on the computation of scattering matrices for each of the profiles and is enhanced in (*48*) to a stable algorithm for an arbitrary number of profiles. The extension of this algorithm to conical diffraction will be outlined in Sect. 4.3. In (*48*), the method is applied to theoretical studies of band gaps of two-dimensional photonic crystals which can be modeled by a stack of rod gratings. The calculation of the matrices of reflection and transmission for each rod grating leads to equations of the form (12) with several right hand sides, but the integral operators are given on a closed curve, the boundary of the rod. Another interesting application is the study of a new kind of diffraction grating in (*49*), the photonic crystal diffraction grating, where the rod gratings have different periods. Electromagnetic results predict in-plane blazing, for instance, which could lead to a break-through in photonics applications. As a generalisation, we present off-plane blazing for the same example in Sect. 5.1.

Additionally to the aforementioned methods and investigations, there have been reams of further investigations on diffraction problems not mentioned here often being the first of its kind. In this way and thanks to the authors creativity, these methods and investigations brought a significantly deeper insight into grating theory and its applications.

3.3. *Modified integral method*

The so-called modified integral method (MIM), introduced in (*32, 38*), uses the same theoretical approach as presented in the previous Sect. 3.2 and hence, is a modification of the 'single equation integral method' IEM. Furthermore, it uses an adapted Nyström collocation method with piecewise constant basis functions for solving the integral equations over the profile, which is a robust and universal technique and can be given parametrised as shown in (*30*). Hence, overhanging profiles are allowed and a uniform discretisation along the arc length of the profile is possible. A regularisation of integrals is used even at corner nodes of a non-smooth boundary, introduced in (*29*). Quadrature is performed by the rectangular rule with single-term corrections for (a) the Green function by accounting for its logarithmic singularity and for (b) the normal derivatives of the Green function by accounting for the profile curvature, respectively. For smooth profiles, this yields an $\mathcal{O}(N^{-3})$–accuracy for diffraction amplitudes and efficiencies of both polarisations. For a faster calculation of the slow converging series of the several kernel functions in equations (12), a convergence acceleration technique is applied according to the Euler method like described in (*50*), for example.

Due to the nature of the boundary method itself, the path of integration for the surface current density coincides with real surfaces of the grating layer boundaries. Hence, the MIM takes all variations of the profile functions into account including the fine structure of the profiles. Since additionally, the MIM also uses the approach to multi-profile gratings mentioned in Sect. 3.2 it can treat bulk and multilayer gratings with real groove profiles in the EUV and X-ray range with a large number of layers including its stray light from random micro-roughness (*32, 33, 51*) which is very important for multilayer applications and is noteworthy for integral methods. Fourier expansion methods, in contrast, represent groove profiles in a distorted form yielding artificial field enhancements (*52*) and a smoothing of edges (*6*). The MIM enables one to deal with

almost all kinds of grating problems, including such difficult cases like the investigation of echelle gratings in low, medium, and very high (up to 1431) diffraction orders (*26*), with the deviation to measured data being less than two percent, a very noteworthy result as well. In addition to the 'conformal' coating type studied in (*47*), a new type of coating called 'non-conformal' layer was introduced in (*53*). The apex of both, the conformal and the non-conformal layers, are translationally displaced normal to the grating plane, whereas the profile of the non-conformal layer is additionally tilted with the apex of the coating profile as pivotal point, so that tapered coatings on the two facets of the echelle are created. As stated in (*53*), it is true that a part of the Green function values on the upper profile for conformal layers can be reused from the lower profile, speeding up the numerical computation. This realisation was already proposed in (*29*) and it has also been implemented in the integral method described in the following Sect. 3.4 from the beginning. However, such a re-use is not possible for non-conformal layers.

Clearly, the MIM can deal with nearly all kinds of grating diffraction problems. Its greatest benefit, however, seems to be the fast treatment of multilayer gratings with real groove profiles in the EUV and X-ray range with a large number of layers including micro-roughness.

3.4. *Integral equation system method with parametrisation*

The algorithm and method (*29–31, 54*), implemented from 1984 to 1986, is the first boundary integral method using a parametrisation of the grating profile from the beginning, whereas the IEM described in Sect. 3.2 started with a discretisation along the x-axis and a parametrisation was implemented later (*47*). This also reflects the name of the method: Integral Equation System Method with Parametrisation (IESMP). Thus, all types of profiles could be treated with the IESMP from the beginning including profiles with vertical side walls and overhangings occurring in the fabrication of holographic gratings by overdevelopment or by underetching of lithographic structures. The first publication of the IESMP (*29*) uses a general operator calculus for describing the extension to overcoated gratings, for the faster solution of multiple coated gratings, and for the treatment of partially overcoated gratings.

For the one-profile case the system of integral equations

$$\begin{aligned} V^+ w - (I + K^+)\tau &= 2u^{\mathrm{in}} \\ cV^- w + (I - K^-)\tau &= 0 \end{aligned} \tag{14}$$

is solved, where for TE polarisation, $c = 1$, $u^{\mathrm{in}} = E_{\mathrm{z}}^{\mathrm{in}}$ and

$$w = \partial_{\mathrm{n}}(E_{\mathrm{z}} - E_{\mathrm{z}}^{\mathrm{in}})^+ = \partial_{\mathrm{n}} E_{\mathrm{z}}^- \ , \ \tau = (E_{\mathrm{z}} - E_{\mathrm{z}}^{\mathrm{in}})^+ = E_{\mathrm{z}}^- \ ,$$

whereas for TM polarisation, $c = \varepsilon_+/\varepsilon_-$, $u^{\mathrm{in}} = B_{\mathrm{z}}^{\mathrm{in}}$ and

$$w = \partial_{\mathrm{n}}(B_{\mathrm{z}} - B_{\mathrm{z}}^{\mathrm{in}})^+ = c^{-1}\partial_{\mathrm{n}} B_{\mathrm{z}}^- \ , \ \tau = (B_{\mathrm{z}} - B_{\mathrm{z}}^{\mathrm{in}})^+ = B_{\mathrm{z}}^- \ .$$

Initially, the arising linear equations were solved by a direct method, later an iterative method (*55*) was used reducing the numerical complexity of the solution to $\mathcal{O}(N^2)$ for smooth profiles.

Additionally, the numerical tools are applied also to single coated gratings, where an alternative method compared to (*28*) leads to an integral equation system similar to equation (14), but with products of operators. This approach needs only the (iterative) solution of the resulting linear equation system and no matrix inversion is necessary speeding up the numerical calculation. Additionally, a part of the Green function values on the upper profile are reused from the lower profile for conformal layers as already mentioned in Sect. 3.3.

Moreover, an efficient summation method for the integral kernels and special treatment of the integrals $V^{\pm}$ having logarithmic singularities (*30, 31*) ensured $\mathcal{O}(N^{-3})$–accuracy of the IESMP for smooth profiles. The summation method consists in a power series representation of the kernel

functions by a polynomial approximation of the coefficients to the fifth order (*31*, Appendix A). Soon, theoretical as well as practical investigations on the effects of grating diffraction have been performed (*56–58*). The IESMP was explained in more detail and compared with other electromagnetic methods and with measurements in (*30, 31*) from infrared to synchrotron radiation applications (*59*).

Further improvements of the IESMP are reported in (*34*) demonstrating the power of the method for echelle gratings with very thin coatings in a high diffraction order. Besides trigonometric functions also splines can now be used as trial functions for the collocation method, which together with a suitable mesh refinement towards profile corners allows to preserve the high convergence rates also for profiles with edges (as e.g. echelles). An iterative solver for the discrete systems was implemented with a preconditioner constructed such that the number of iterations is almost independent on the number of unknowns. This reduces the numerical complexity to $\mathcal{O}(N^2)$ in all cases including problems with high wave numbers (large ratios of period to wavelength) which formerly, due to the oscillatory behaviour of the kernel functions, caused serious troubles for the iterative solver. Another important improvement is the implementation of an exponentially convergent quadrature rule with graded meshes for integrals with weakly singular or almost singular kernels, occurring in the treatment of corners or very thin coatings. Therefore, a summation algorithm for the integral kernels based on Ewalds method is used (*60*) which is better suited to small moduli $|y|$, occurring more frequently in the new quadrature rule due to the graded meshes. Altogether, the improvements resulted in one of the most accurate and fastest diffraction methods available, especially for large numbers of discretisation points necessary for applications with large ratios of grating period to wavelength, for example.

4. Integral equations for conical diffraction

The integral method for in-plane diffraction has been implemented very early, whereas conical diffraction of a finitely conducting interface has not been tackled for a long time. This was one of the real deficiencies of the method. Other methods like the differential, Fourier modal, coordinate transformation, and finite element method implemented conical diffraction much earlier and often from the introduction of the particular method. The conical diffraction for a perfectly conducting grating is relatively simple and can be determined from the two fundamental polarisations for a modified in-plane diffraction case (cf. e.g. (*28*, Sect. 3.7)). A first theoretical derivation of the integral method for conical diffraction of a finitely conducting interface has been given in (*40*) as referenced in (*7*), but has not been published otherwise and seemed not to be implemented. A boundary integral method for conical diffraction of three dimensional finitely conducting lithographic grating structures has been published in (*61, 62*). However, an electrical engineer's approximate approach (*63*) has been used to avoid the singularity issue and the mathematical problems connected therewith, rather than the rigorous approach, addressed here. Other interesting integral methods dealing with conical diffraction are e.g. (*64, 65*), avoiding the evaluation of the quasi-periodic Greens functions by Neumann-to-Dirichlet maps.

In this section, we present the generalisation of Maystre's in-plane integral formulation to the conical diffraction case. Based on the integral equations for one interface given in Sect. 4.1, it is rather straightforward to extend the method to gratings with stacks of interfaces in a common description. This is demonstrated in Sects. 4.2 – 4.5 for multilayer gratings with separated interfaces of arbitrary finite conductivity, including photonic crystal and plasmonic diffraction gratings. The extension of this approach to the other interesting case of stacks of possibly interpenetrating layers has been studied theoretically and implemented quite recently. It is actually tested and will be discussed in a forthcoming paper.

4.1. *Gratings with one profile*

At first a formulation for one profile is considered (cf. Sect. 2 for the notation). It extends the approach described in Sect. 3.2 and was introduced in (*35*). Using the single layer potential representations (11) for E_z, B_z in the bottom layer G_- (cf. Figure 1), the transmission conditions (4) lead to a system of integral equations for the unknown densities w and τ on Γ:

$$\begin{aligned} \Big(\frac{\varepsilon_-\kappa_+^2}{\varepsilon_+\kappa_-^2}V^+(I-L^-)+(I+K^+)V^-\Big)w-\sin\phi\,\frac{\kappa_-^2-\kappa_+^2}{\kappa_-^2}\,V^+\partial_t V^-\tau &= -2E_z^{\mathrm{in}}\,,\\ \sin\phi\,\frac{\kappa_-^2-\kappa_+^2}{\kappa_-^2}\,V^+\partial_t V^- w+\Big(\frac{\mu_-\kappa_+^2}{\mu_+\kappa_-^2}\,V^+(I-L^-)+(I+K^+)V^-\Big)\tau &= -2B_z^{\mathrm{in}}\,, \end{aligned} \tag{15}$$

where the boundary integrals are defined in equation (13). Obviously, the main theoretical and numerical difficulty is the product $V^+\partial_t V^-$ of three operators. Formal integration by parts gives

$$V^+\partial_t\varphi=\int_\Gamma \partial_t\varphi(Q)\,\Psi_{\kappa_+,\alpha}(P-Q)\,\mathrm{d}\sigma_Q=-\int_\Gamma \varphi(Q)\,\partial_{t(Q)}\Psi_{\kappa_+,\alpha}(P-Q)\,\mathrm{d}\sigma_Q\,.$$

The integral on the right, denoted by $H^+\varphi$, does not exist in usual sense, since the tangential derivative $\partial_{t(Q)}\Psi_{\omega\kappa_0,\alpha}(P-Q)$ has a strong singularity for $Q\to P$. But it can be interpreted as singular integral

$$H^+\varphi(P)=\lim_{\delta\to0}\int_{\Gamma\setminus\Gamma(P,\delta)}\varphi(Q)\,\partial_{t(Q)}\Psi_{\kappa_+,\alpha}(P-Q)\,\mathrm{d}\sigma_Q\,, \tag{16}$$

where $\Gamma(P,\delta)$ is the sub-arc of Γ of length 2δ with the mid point P. Therefore, one has to apply mathematical and numerical methods for singular integral equations in order to analyse and solve the system (15). Roughly spoken, in the case of a smooth interface Σ the system is solvable and provides a solution of the conical diffraction problem if $\varepsilon_-\neq-\varepsilon_+$ and $\mu_-\neq-\mu_+$. If the profile has corners, then the solvability of the system (15) can be guaranteed if the ratios $\varepsilon_-/\varepsilon_+$ and μ_-/μ_+ do not belong to a closed interval $[\rho,\rho^{-1}]$ for some $\rho<-1$ depending on the angles at corners of Σ.

These results are valid also for rod gratings, where in contrast to the relief gratings considered above, the d-periodic profile Σ is not continuous, but consists of a union of non-intersecting closed curves $\{\Gamma+nd(1,0)\}_{n\in\mathbb{Z}}$. Then the dielectric region $G_+\times\mathbb{R}$ is unbounded also for $y\to-\infty$, and the region $G_-\times\mathbb{R}$ contains rods of material coefficients ε_-,μ_-. Consequently, the differential formulation (3), (4) for E_z, B_z holds, only the second radiation condition in equation (5) changes to

$$(E_z,B_z)=\sum_{n\in\mathbb{Z}}(E_n^-,B_n^-)\exp(\,\mathrm{i}(\alpha_n x-\beta_n^+ y)),\quad y\le-H. \tag{17}$$

Representing E_z, B_z in the interior of Γ as single layer potentials (11), conditions (4) lead, as before, to the integral equation system (15), but now the integrals are defined over the closed curve Γ.

Moreover, trigonometric collocation methods for solving system (15) converge under the assumptions made above. Some numerical results for gratings with continuous interface are reported in (*36*). For profiles with corners the algorithm uses a hybrid spline-trigonometric method on graded meshes. The obtained results confirm that the code is accurate and efficient for solving off-plane diffraction problems including high-conductive gratings, surfaces with edges, real profiles, and gratings working at short wavelengths.

4.2. *Multi-profile gratings with separated interfaces*

Let us now consider a multilayer diffraction grating with period d formed by a stack of N relief and/or rod gratings characterized by grating profiles Σ_j, $j = 0, \dots, N-1$.

PLEASE INSERT FIGURE 2 ABOUT HERE

More precisely, the structure consists of material layers which are separated by continuous profiles and may contain rod gratings. The different media are numbered from top to bottom, see Figure 2, G_0 and G_N are the semi-infinite top and bottom layers. To apply a scattering matrix approach we assume that the interfaces $\Sigma_0, \dots, \Sigma_{N-1}$ between the $N+1$ homogeneous material domains $G_0, \dots, G_N$ are separated, i.e. between adjacent interfaces Σ_j and Σ_{j-1} there exists a strip $\{u_j < y < d_{j-1}\}$ not crossing the interfaces. The structure of the multi-profile grating is characterized by the permittivity and permeability functions $\varepsilon(x,y)$ and $\mu(x,y)$, which are constant on the domains G_j. Its values in G_0 and G_N are denoted by ε_0, ε_N and μ_0, μ_N, respectively. Further we denote

$$\kappa_0^2 = \varepsilon_0\mu_0 \cos^2\phi\,, \quad \kappa_N^2 = \varepsilon_N\mu_N - \varepsilon_0\mu_0 \sin^2\phi\,.$$

As in the case of one interface the z-components $E_{\rm z}$, $B_{\rm z} = (\mu_0/\varepsilon_0)^{1/2} H_{\rm z}$ satisfy Helmholtz equations

$$\left(\Delta + \omega^2(\varepsilon\mu - \varepsilon_0\mu_0 \sin^2\phi)\right) E_{\rm z} = \left(\Delta + \omega^2(\varepsilon\mu - \varepsilon_0\mu_0 \sin^2\phi)\right) B_{\rm z} = 0 \tag{18}$$

in the domains G_j and the transmission conditions at the interfaces Σ_j

$$\left[E_{\rm z}\right]_{\Sigma_j} = \left[B_{\rm z}\right]_{\Sigma_j} = \left[\frac{\varepsilon\,\partial_{\rm n}E_{\rm z}}{\kappa^2} + \varepsilon_0 \sin\phi \frac{\partial_{\rm t}B_{\rm z}}{\kappa^2}\right]_{\Sigma_j} = \left[\frac{\mu\,\partial_{\rm n}B_{\rm z}}{\kappa^2} - \mu_0 \sin\phi \frac{\partial_{\rm t}E_{\rm z}}{\kappa^2}\right]_{\Sigma_j} = 0\,. \tag{19}$$

The light is incident from G_0 and we are interested in the Rayleigh coefficients $E_n^{\pm}, B_n^{\pm}$ of the series expansions

$$\begin{aligned} (E_{\rm z}, B_{\rm z}) &= (E_{\rm z}^{\rm in}, B_{\rm z}^{\rm in}) + \sum_{n\in\mathbb{Z}} (E_n^+, B_n^+) \exp(\,{\rm i}(\alpha_n x + \beta_n^{(0)} y)), \quad && y \geq H, \\ (E_{\rm z}, B_{\rm z}) &= \sum_{n\in\mathbb{Z}} (E_n^-, B_n^-) \exp(\,{\rm i}(\alpha_n x - \beta_n^{(N)} y)), && y \leq -H, \end{aligned} \tag{20}$$

where $\beta_n^{(j)} = (\omega^2\kappa_j^2 - \alpha_n^2)^{1/2}$ and the half spaces $\{y \geq H\}$ and $\{y \leq -H\}$ are contained in the semi-infinite layers G_0 and G_N, respectively.

4.3. *Recursive algorithm*

We study the off-plane diffraction for gratings with separated interfaces using the algorithm proposed by Maystre (*48*) for the in-plane case. In any of the strips $\{u_j < y < d_{j-1}\}$ the functions ε and μ take constant values and we introduce its wave number κ_j by

$$\kappa_j^2 = \varepsilon\mu - \varepsilon_0\mu_0 \sin^2\phi\,.$$

As quasiperiodic solutions of the Helmholtz equation

$$(\Delta + \omega^2\kappa_j^2)\, u = 0$$

in the strips $\{u_j < y < d_{j-1}\}$ between Σ_j and Σ_{j-1}, $j = 1, \ldots, N-1$, the functions E_z, B_z are smooth and bounded. Hence, for $y \in (u_j, d_{j-1})$

$$(E_z, B_z) = \sum_{n\in\mathbb{Z}} \Big((a_n^j, c_n^j) \exp(-\mathrm{i}\beta_n^{(j)} y) + (b_n^j, d_n^j) \exp(\mathrm{i}\beta_n^{(j)} y) \Big) \exp(\mathrm{i}\alpha_n x) \text{ with } \beta_n^{(j)} = (\omega^2\kappa_j^2 - \alpha_n^2)^{1/2} .$$

Assign to each profile Σ_j a characteristic y-coordinate y_j, for example $y_j = Y_j(0)$ for a given parametrisation $(X_j(t), Y_j(t))$ of the profile Σ_j. Recall that $y_0 > y_1 > \ldots > y_{N-1}$. Using the notation

$$\begin{aligned} (A_n^j, C_n^j) &= \exp(-\mathrm{i}\beta_n^{(j)} y_j)(a_n^j, c_n^j) , & (B_n^j, D_n^j) &= \exp(\mathrm{i}\beta_n^{(j)} y_j)(b_n^j, d_n^j) , \\ (\mathcal{A}_n^j, \mathcal{C}_n^j) &= \exp(-\mathrm{i}\beta_n^{(j+1)} y_j)(a_n^{j+1}, c_n^{j+1}) , & (\mathcal{B}_n^j, \mathcal{D}_n^j) &= \exp(\mathrm{i}\beta_n^{(j+1)} y_j)(b_n^{j+1}, d_n^{j+1}) , \end{aligned} \tag{21}$$

the field in $\{u_j < y < d_{j-1}\}$ above Σ_j is given by

$$(E_z, B_z) = \sum_{n\in\mathbb{Z}} [(A_n^j, C_n^j) \exp(-\mathrm{i}\beta_n^{(j)}(y - y_j)) + (B_n^j, D_n^j) \exp(\mathrm{i}\beta_n^{(j)}(y - y_j))] \exp(\mathrm{i}\alpha_n x), \tag{22}$$

whereas in $\{u_{j+1} < y < d_j\}$ below Σ_j

$$(E_z, B_z) = \sum_{n\in\mathbb{Z}} [(\mathcal{A}_n^j, \mathcal{C}_n^j) \exp(-\mathrm{i}\beta_n^{(j+1)}(y - y_j)) + (\mathcal{B}_n^j, \mathcal{D}_n^j) \exp(\mathrm{i}\beta_n^{(j+1)}(y - y_j))] \exp(\mathrm{i}\alpha_n x). \tag{23}$$

The terms $(A_n^j, C_n^j) \exp(-\mathrm{i}\beta_n^{(j)}(y - y_j)) \exp(\mathrm{i}\alpha_n x)$ and $(\mathcal{B}_n^j, \mathcal{D}_n^j) \exp(\mathrm{i}\beta_n^{(j+1)}(y - y_j)) \exp(\mathrm{i}\alpha_n x)$ correspond to incident waves on the profile Σ_j, whereas $(B_n^j, D_n^j) \exp(-\mathrm{i}\beta_n^{(j)}(y - y_j)) \exp(\mathrm{i}\alpha_n x)$ and $(\mathcal{A}_n^j, \mathcal{C}_n^j) \exp(\mathrm{i}\beta_n^{(j+1)}(y - y_j)) \exp(\mathrm{i}\alpha_n x)$ represent the diffracted waves. Thus, the coefficients in equations (22) and (23) are linked by the reflection and transmission matrices of the grating having only the interface Σ_j. For a compact notation we introduce the infinite coefficient vectors

$$\boldsymbol{A}_j = (\ldots, A_{-1}^j, A_0^j, A_1^j, \ldots, C_{-1}^j, C_0^j, C_1^j, \ldots)^T , \ \boldsymbol{B}_j = (\ldots, B_{-1}^j, B_0^j, B_1^j, \ldots, D_{-1}^j, D_0^j, D_1^j, \ldots)^T ,$$

and similarly $\mathcal{A}_j$ and $\mathcal{B}_j$, since E_z and B_z cannot be treated independently for conical diffraction. Then equations (21) can be written in the form

$$\mathcal{A}_{j-1} = \boldsymbol{\gamma}_j^{-1} \boldsymbol{A}_j , \ \mathcal{B}_{j-1} = \boldsymbol{\gamma}_j \boldsymbol{B}_j , \tag{24}$$

with the infinite diagonal matrix

$$\boldsymbol{\gamma}_j = \mathrm{diag}(\ldots, \exp(\mathrm{i}\beta_{-1}^{(j)} h_j), \exp(\mathrm{i}\beta_0^{(j)} h_j), \exp(\mathrm{i}\beta_1^{(j)} h_j), \ldots, \exp(\mathrm{i}\beta_{-1}^{(j)} h_j), \exp(\mathrm{i}\beta_0^{(j)} h_j), \ldots),$$

with

$$h_j = y_{j-1} - y_j > 0 .$$

Denoting by $\mathbf{r}_j, \mathbf{t}_j$ the (infinite) reflection and transmission matrices of the grating with profile Σ_j for illumination from above and by $\mathbf{r}'_j, \mathbf{t}'_j$ the corresponding matrices for illumination of Σ_j from below, for $j = 1, \ldots, N-2$ the coefficient vectors are linked by the relations

$$\boldsymbol{B}_j = \mathbf{r}_j \boldsymbol{A}_j + \mathbf{t}'_j \mathcal{B}_j , \quad \mathcal{A}_j = \mathbf{t}_j \boldsymbol{A}_j + \mathbf{r}'_j \mathcal{B}_j . \tag{25}$$

The same relation for $j = 0$ is obtained from equation (20) written as

$$(E_z, B_z) = (A_0^0, C_0^0)\exp(\,\mathrm{i}\alpha x - \mathrm{i}\beta(y - y_0)) + \sum_{n\in\mathbb{Z}}(B_n^0, D_n^0)\exp(\mathrm{i}\beta_n^{(0)}(y - y_0))\exp(\mathrm{i}\alpha_n x)\,.$$

The integral method for calculating the reflection and transmission matrices for one-profile gratings will be considered in the next subsection. Here we provide the formulas for solving the multi-profile problem with given input $\boldsymbol{A}_0$ and vanishing $\mathcal{B}_{N-1}$, which can be derived similar to (*48*). The idea is to look for a recursion for the operators $\mathbf{R}_j, \mathbf{T}_j$ such that

$$\boldsymbol{B}_j = \mathbf{R}_j\boldsymbol{A}_j\,,\ \mathcal{A}_{N-1} = \mathbf{T}_j\boldsymbol{A}_j\,,\quad j = N-1,\dots,0.$$

By writing equation (20) as

$$(E_z, B_z) = \sum_{n\in\mathbb{Z}}(\mathcal{A}_n^{N-1}, \mathcal{C}_n^{N-1})\exp(-\mathrm{i}\beta_n^{(N)}(y - y_{N-1}))\exp(\mathrm{i}\alpha_n x)\,,\quad y < -H,$$

one derives the initial values

$$\mathbf{R}_{N-1} = \mathbf{r}_{N-1}\,,\ \mathbf{T}_{N-1} = \mathbf{t}_{N-1}\,. \tag{26}$$

As in (*48*) relations (25) and (24) lead to the recursion formulas for $j = N-1,\dots,1$

$$\begin{aligned}\mathbf{R}_{j-1} &= \mathbf{r}_{j-1} + \mathbf{t}'_{j-1}\boldsymbol{\gamma}_j\mathbf{R}_j\big(\mathbf{I} - \boldsymbol{\gamma}_j\mathbf{r}'_{j-1}\boldsymbol{\gamma}_j\mathbf{R}_j\big)^{-1}\boldsymbol{\gamma}_j\mathbf{t}_{j-1}\,,\\ \mathbf{T}_{j-1} &= \mathbf{T}_j\big(\mathbf{I} - \boldsymbol{\gamma}_j\mathbf{r}'_{j-1}\boldsymbol{\gamma}_j\mathbf{R}_j\big)^{-1}\boldsymbol{\gamma}_j\mathbf{t}_{j-1}\,,\end{aligned} \tag{27}$$

and finally one gets the desired coefficient vectors

$$\boldsymbol{B}_0 = \mathbf{R}_0\boldsymbol{A}_0\,,\ \mathcal{A}_{N-1} = \mathbf{T}_0\boldsymbol{A}_0\,. \tag{28}$$

4.4. *Determination of the scattering matrices*

In order to find the scattering matrices $\mathbf{r}_j, \mathbf{t}_j$ and $\mathbf{r}'_j, \mathbf{t}'_j$ for given $j = 0,\dots,N-1$, one has to solve one-profile grating problems with incident waves from above and below for the profile Σ_j shifted by $-y_j$. More precisely, one has to find the Rayleigh coefficients of the diffracted fields for input waves with z-components

$$\begin{pmatrix}u_\delta^+\\ v_\delta^+\end{pmatrix} = \begin{pmatrix}1-\delta\\ \delta\end{pmatrix}\exp(\,\mathrm{i}\alpha_n x - \mathrm{i}\beta_n^{(j)} y)\,,\ \begin{pmatrix}u_\delta^-\\ v_\delta^-\end{pmatrix} = \begin{pmatrix}1-\delta\\ \delta\end{pmatrix}\exp(\,\mathrm{i}\alpha_n x + \mathrm{i}\beta_n^{(j+1)} y)\,,\ \delta = 0, 1\,. \tag{29}$$

We choose the indices $n \in [m, M]$ such that at least all propagating modes for all one-profile gratings are covered, i.e. we require that $\beta_n^{(j)} \notin \mathbb{R}$ for all $n \notin [m, M]$ and j. Then all matrices appearing in the recursion algorithm (26 - 28) are $\mathcal{M}\times\mathcal{M}$ matrices with $\mathcal{M} = 2(M - m + 1)$. If we use the ordering

$$\boldsymbol{A}_j = (A_m^j,\dots,A_M^j, C_m^j,\dots,C_M^j)^T\,,\ \boldsymbol{B}_j = (B_m^j,\dots,B_M^j, B_m^j,\dots,B_M^j)^T\,,\ \dots$$

of the components of the coefficient vectors $\boldsymbol{A}_j,\dots$, then $\boldsymbol{\gamma}_j$ is a diagonal matrix of the form

$$\boldsymbol{\gamma}_j = \mathrm{diag}(\exp(\mathrm{i}\beta_m^{(j)}h_j),\dots,\exp(\mathrm{i}\beta_M^{(j)}h_j),\exp(\mathrm{i}\beta_m^{(j)}h_j),\dots,\exp(\mathrm{i}\beta_M^{(j)}h_j))\,.$$

First we consider the calculation of the scattering matrices for a continuous interface Σ_j. It separates two layers and the one-profile problem corresponds to the situation depicted in Figure 1. We denote the semi-infinite domains above and below the profile $\Sigma = \{(x, y - y_j) : (x, y) \in \Sigma_j\}$ by $G_\pm$ and by $\varepsilon_\pm$, $\mu_\pm$ the material coefficients above and below Σ, respectively. Thus we keep the notation of Sect. 4.1, but the difference to the problem there is the occurrence of different incident waves from above and below and the fixed values ε_0 and μ_0 in condition (19).

For illumination from above one has to solve the following problem: Setting

$$E_{\rm z} = \begin{cases} u_+ + u_\delta^+ \text{ in } & G_+\,, \\ u_- \quad \text{in } & G_-\,, \end{cases} \qquad B_{\rm z}(x,y) = \begin{cases} v_+ + v_\delta^+ \text{ in } & G_+, \\ v_- \quad \text{in } & G_-, \end{cases}$$

find α-quasiperiodic solutions of the Helmholtz equations

$$\text{in } G_+ \qquad \Delta u_+ + \omega^2\kappa_+^2 u_+ = \Delta v_+ + \omega^2\kappa_+^2 v_+ = 0\,, \tag{30}$$

$$\text{in } G_- \qquad \Delta u_- + \omega^2\kappa_-^2 u_- = \Delta v_- + \omega^2\kappa_-^2 v_- = 0\,, \tag{31}$$

where now $\kappa_\pm^2 = \varepsilon_\pm\mu_\pm - \varepsilon_0\mu_0\sin^2\phi$. From equation (19) one gets the jump conditions on Σ

$$\begin{aligned} u_- = u_+ + u_\delta^+\,,\ \frac{\varepsilon_-\,\partial_{\rm n} u_-}{\kappa_-^2} - \frac{\varepsilon_+\partial_{\rm n}(u_+ + u_\delta^+)}{\kappa_+^2} &= \frac{\varepsilon_0\sin\phi(\kappa_-^2 - \kappa_+^2)}{\kappa_+^2\kappa_-^2}\,\partial_{\rm t} v_-\,, \\ v_- = v_+ + v_\delta^+\,,\ \frac{\mu_-\partial_{\rm n} v_-}{\kappa_-^2} - \frac{\mu_+\partial_{\rm n}(v_+ + v_\delta^+)}{\kappa_+^2} &= -\frac{\mu_0\sin\phi(\kappa_-^2 - \kappa_+^2)}{\kappa_+^2\kappa_-^2}\,\partial_{\rm t} u_-\,. \end{aligned} \tag{32}$$

For illumination from below we set

$$E_{\rm z} = \begin{cases} u_+ \quad \text{in } & G_+\,, \\ u_- + u_\delta^- \text{ in } & G_-\,, \end{cases} \qquad B_{\rm z} = \begin{cases} v_+ \quad \text{in } & G_+, \\ v_- + v_\delta^- \text{ in } & G_-. \end{cases}$$

The α-quasiperiodic functions $u_\pm, v_\pm$ have to satisfy the Helmholtz equations (30), (31) and the transmission conditions

$$\begin{aligned} u_- + u_\delta^- = u_+\,,\ \frac{\varepsilon_-\partial_{\rm n}(u_- + u_\delta^-)}{\kappa_-^2} - \frac{\varepsilon_+\,\partial_{\rm n} u_+}{\kappa_+^2} &= \frac{\varepsilon_0\sin\phi(\kappa_-^2 - \kappa_+^2)}{\kappa_+^2\kappa_-^2}\,\partial_{\rm t} v_+\,, \\ v_- + v_\delta^- = v_+\,,\ \frac{\mu_-\partial_{\rm n}(v_- + v_\delta^-)}{\kappa_-^2} - \frac{\mu_+\partial_{\rm n} v_+}{\kappa_+^2} &= -\frac{\mu_0\sin\phi(\kappa_-^2 - \kappa_+^2)}{\kappa_+^2\kappa_-^2}\,\partial_{\rm t} u_+\,. \end{aligned} \tag{33}$$

Choosing as before u_-, v_- as single layer potentials (11), we derive from equations (32) and (33) the system of singular integral equations

$$\begin{aligned} \Big(\frac{\varepsilon_-\kappa_+^2}{\varepsilon_+\kappa_-^2}V^+(I - L^-) + (I + K^+)V^-\Big)w + \sin\phi\,\frac{\varepsilon_0(\kappa_-^2 - \kappa_+^2)}{\varepsilon_+\kappa_-^2}\,H^+V^-\tau &= U\,, \\ -\sin\phi\,\frac{\mu_0(\kappa_-^2 - \kappa_+^2)}{\mu_+\kappa_-^2}\,H^+V^- w + \Big(\frac{\mu_-\kappa_+^2}{\mu_+\kappa_-^2}\,V^+(I - L^-) + (I + K^+)V^-\Big)\tau &= V\,, \end{aligned} \tag{34}$$

with the singular integral H^+ defined in equation (16). For illumination from above the right-hand side is given by

$$U = -2\,u_\delta^+\,,\ V = -2\,v_\delta^+\,,$$

whereas in the case of illumination from below

$$U = \frac{\varepsilon_-\kappa_+^2}{\varepsilon_+\kappa_-^2}\, V^+\partial_{\rm n} u_\delta^- - (I + K^+)u_\delta^- + \sin\phi\frac{\varepsilon_0(\kappa_-^2 - \kappa_+^2)}{\varepsilon_+\kappa_-^2}\, H^+ v_\delta^- \,,$$

$$V = \frac{\mu_-\kappa_+^2}{\mu_+\kappa_-^2}\, V^+\partial_{\rm n} v_\delta^- - (I + K^+)v_\delta^- - \sin\phi\frac{\mu_0(\kappa_{j+1}^2 - \kappa_j^2)}{\mu_+\kappa_-^2}\, H^+ u_\delta^- \,.$$

In the case of a rod grating with a discontinuous profile the domain G_- is bounded. Using the single layer potential ansatz in G_-, illumination from above is treated as before. Illumination from below can be treated by setting

$$E_{\rm z} = \begin{cases} u_+ + u_\delta^- & \text{in} \quad G_+\,, \\ u_- & \text{in} \quad G_-\,, \end{cases} \qquad B_{\rm z} = \begin{cases} v_+ + v_\delta^- & \text{in} \quad G_+, \\ v_- & \text{in} \quad G_-, \end{cases}$$

which results in the system (34) with the right-hand side

$$U = -2\, u_\delta^- \,,\; V = -2\, v_\delta^- \,.$$

Thus, in all considered cases the system (34) can be used to determine the scattering matrices. Moreover, it can be shown that the solvability of system (34) does not depend on ε_o and μ_o. Similar to the system (15) the equations are solvable, if the ratios $\varepsilon_-/\varepsilon_+$ and μ_-/μ_+ do not belong to an interval on the negative axis. Thus the applicability of the algorithm is independent of the incidence angles θ and ϕ as well as of the polarisation.

4.5. *Numerical computation of the scattering matrices*

The numerical approximation of the scattering matrices is performed by an extension of the method reported in (*36*). The integral operators in the system (34) are discretized by collocation with trigonometric polynomials as trial functions in case of a smooth profile Γ_j, which gives approximation order $\mathcal{O}(N^{-3})$, where N is the number of discretisation points. Here one has to compute the fundamental solutions and their normal and tangential derivatives, which is rather involved, only for the discretisation points. To retain a similar high convergence rate also for profiles with corners, it is necessary to choose trial functions better adapted to the singularities of the solution near corner points, which are in general of the form $\mathcal{O}(r^{-\rho})$, $\rho < 1$, r is the distance to a corner point. As discussed in (*34*), one good choice for solving the integral equations of classical diffraction are splines as trial functions and mesh refinement towards the profile corners. However, the accurate computation of the integrals applied to splines requires high order quadrature rules and therefore the computation of the fundamental solutions and their derivatives for a large number of quadrature points. To combine the efficient computation of the integrals for trigonometric polynomials with the good approximation properties of piecewise polynomials on graded meshes near edges we use a hybrid trigonometric-spline collocation method, where only a fixed number of trigonometric polynomials is replaced by splines supported in the vicinity of corner points. More details of this approach and some numerical results for one-profile gratings are given in (*36*).

Compared to the case of one-profile gratings the computation of the scattering matrix requires to solve these equations with several right-hand sides, which correspond to the illumination modes (29) for a finite number of integers n and $\delta = 0, 1$. The advantage of the proposed integral formulation is that, after having discretised system (34) and determined the LU factorisation of the discrete matrix, which is the most time-consuming part of the algorithm, the solutions of the system with the various right-hand sides can be found immediately. So, the computing time to determine the scattering matrix of a given profile is comparable to a simple solution of the equation using a direct solver.

5. Examples

5.1. *Blazing at a photonic crystal diffraction grating in conical mounting*

Our first example applies the new theory from Sect. 4.2 and compares simulations of blazing effects at a photonic crystal diffraction grating (cf. Figure 3) made from dielectric rods with refractive index $n = 3$ in air presented in (*49*).

PLEASE INSERT FIGURE 3 ABOUT HERE

The configuration consists of two parts: a rod grating of period D in -1^{st} order Littrow mounting and an underlying two-dimensional photonic crystal with hexagonal symmetry and period $d = 1$. Littrow mount of -1^{st} order is characterised by the condition $\sin\theta_{\text{L}} = \lambda/(2D)$, with θ_{L} being the Littrow angle. The grating and the photonic crystal have infinite extensions in the periodic x-direction whereas the extension of the photonic crystal in y-direction is limited to $m_{\text{PhC}} = 6$ grids separated by a distance $h = \frac{d}{2}3^{1/2}$, the same distance, the rod grating is separated from the photonic crystal. The grating and the photonic crystal are constructed such that the photonic crystal has a band gap in s–polarisation for wavelengths λ, the grating can blaze for. Then the photonic crystal acts as lossless mirror and 100% efficiency in one diffraction order is possible. The radius of the photonic crystal rods is $r_{\text{PhC}} = 0.2$ and the period of the rod grating is chosen to be $D = 2d$, corresponding to the results presented in Figure 2 of (*49*). We verified all these simulations with various radii for the grating rods.

PLEASE INSERT FIGURE 4 ABOUT HERE

Then the radius of the grating rods has been fixed to be $R_{\text{g}} = 0.15$ possessing a strong blazing effect for in–plane diffraction. To check for a blazing effect also in conical mounting, Figure 4 presents efficiency results for the -1^{st} diffraction order for s–polarisation incidence with $\theta = \theta_{\text{L}}$ but $\phi = 10°$. Obviously, the efficiency is decreased by a small amount due to the deviation of directions between s–polarisation and rods. This has been compensated in Figure 5 by setting the polarisation angle $\delta^{\text{in}} = 80°$ remembering that s–polarisation corresponds to $\delta^{\text{in}} = 90°$.

PLEASE INSERT FIGURE 5 ABOUT HERE

Then, the -1^{st} diffraction order reaches 100% again and hence, we have demonstrated a blazing effect also in conical mounting. Let us remark that also other geometries, like rhomboids instead of the rods for the grating or for the photonic crystal can be considered – and the effects are quite similar.

5.2. *Stacked plasmonic gratings in conical incidence and convergence behaviour*

The excellent convergence of the new theory from Sect. 4.2 is especially demonstrated for the case of stacked metallic plasmonic gratings for conical incidence since convergence for conventional gratings with conical incidence has already been presented in (*36*). In (*66*) an example is presented using a plasmonic multilayer structure consisting of two stacked plasmonic gratings of equal period $d = 500\,\text{nm}$ and thickness $t = 50\,\text{nm}$ with a half pitch shift between the two gratings and a separation distance of $w = 20\,\text{nm}$. The slits S_2 of the bottom grating are centered to be in the middle of the metal rods of the upper grating, and vice versa. All metal rods consist of silver and have a rectangle profile. The widths of the slits are: $S_1 = 250\,\text{nm}$ and $S_2 = 40\,\text{nm}$. The proposed structure forms rectangular metal/insulator/metal cavities and a waveguide with an air gap of $w = 20\,\text{nm}$ between the gratings.

In the following we show similar properties with elliptical silver rods as shown in Figure 6 instead of rectangular ones.

PLEASE INSERT FIGURE 6 ABOUT HERE

To achieve a similar pronounced resonance peak as for the rectangle profile, the structure is optimised, resulting in $S_1 = 150\,\text{nm}$, $S_2 = 50\,\text{nm}$, and $w = 10\,\text{nm}$ for the elliptical rods. Figure 7 presents the in-plane TM polarisation angle dependent zero order reflection of the two stacked plasmonic grating structures for $\lambda = 785\,\text{nm}$ showing a similar behaviour for elliptical and rectangular silver rods.

PLEASE INSERT FIGURE 7 ABOUT HERE

Interestingly, the pronounced resonance peak at about $\theta = 34°$ disappears if one switches over to conical incidence. This is demonstrated in Figure 8 presenting angle dependent zero order reflection for the same structures in conical incidence with $\phi = 30°$ for two polarisation angles $\delta^{\text{in}} = 90°$ and $\delta^{\text{in}} = 52°$. None of the polarisations is able to produce a similar pronounced resonance peak as the in-plane TM polarisation incidence.

PLEASE INSERT FIGURE 8 ABOUT HERE

Our aim is not to discuss the reasons for the disappeared resonance peak, rather we show the excellent efficiency convergence of the new theory of Sects. 4.2 – 4.5 in Figure 9, especially for the above investigated silver structures in conical incidence. The solid curve is for elliptical silver rods, whereas the dashed curve stands for rectangular silver rods.

PLEASE INSERT FIGURE 9 ABOUT HERE

The data documents a convergence according to N^{-3} meaning that a doubling of N reduces the error by a factor of 1/8. Obviously, the errors are smaller for the smooth elliptical rods than for rectangular ones whereas the convergence rate is the same. An accuracy of 10^{-4} for the efficiency is easily achieved with $N = 50$ discretisation points for elliptical rods, whereas for rectangular rods, about $N = 300$ discretisation points are necessary. Nevertheless, both cases take only a fraction of a second up to a few seconds on an usual PC. The CPU times for the above example on an Intel® Core™ 2 Duo P8400 Processor @ 2.26 GHz are given in Table 1.

PLEASE INSERT TABLE 1 ABOUT HERE

5.3. *Blazed diffraction grating in conical incidence*

Our third example applies the theory from Sect. 4.1 and deals with a blazed transmission grating in conical diffraction for the ratio of period to wavelength approaching 180. As mentioned in the introduction Sect. 1, the LLGA is used to model a kinoform DOE for the correction of longitudinal and transverse chromatic aberrations in broadband optical systems such as photographic lenses, head mounted displays or infrared lenses. Consequently, the grating represents a local zone width of the kinoform. Due to the necessary broad visible spectrum from $\lambda_0 = 400\,\text{nm}$ to $\lambda_0 = 700\,\text{nm}$, the refractive power may not be strong and thus the minimal zone width of the kinoform becomes large. In typical cases, the zone width d exceeds a value of $80\,\mu\text{m}$, in rare cases the smallest zone width is $d \geq 20\,\mu\text{m}$. Kinoforms are usually characterised by a blazed surface-relief profile. The groove depth $h = \lambda_0/(n_- - 1)$ is determined by the design wavelength $\lambda_0 = 550\,\text{nm}$ and n_- the refractive index of the kinoform material PMMA with $n_-(\lambda_0) = 1.49357$ and hence $h = 1114\,\text{nm}$.

In (*67*), several scalar approximations for the diffraction efficiency η as a function of various parameters are compared with rigorous electromagnetic calculations.

PLEASE INSERT FIGURE 10 ABOUT HERE

In Figure 10 we present the dependency of the 1st order diffraction efficiency for unpolarised light in transmission on the conical angle ϕ with fixed in-plane angle $\theta = 0°$ and for two zone widths $d = 20\,\mu\text{m}$ and $d = 80\,\mu\text{m}$ for the three wavelengths $\lambda_0 = 550\,\text{nm}$, $\lambda = 650\,\text{nm}$, $\lambda = 450\,\text{nm}$. This is compared with the scalar analytical diffraction efficiency expression (4) of (*67*) by substituting θ by ϕ. Please note, that all efficiencies are parts of transmitted light which is assumed to be 100%. In other words, reflected light is not considered here as it does not directly influence the image of the lens and can be reduced by anti-reflection coatings, for example.

Comparing the results for conical incidence in Figure 10 with the results in Figures 7–9 of (*67*) for in-plane incidence ($\eta_1(\theta)$ and $\phi = 0°$), we observe a quite similar behaviour. Only for red light, corresponding to $\lambda = 650\,\text{nm}$, the efficiency is better by a few percentages for conical incidence compared to in-plane incidence.

Let us remark that the presented method can likewise treat larger grating periods of $d = 150\,\mu\text{m}$ or $d = 200\,\mu\text{m}$ with wavelengths in the visible spectrum as shown in (*67*), for example.

Also scattering investigations with measured or simulated profiles of surfaces presented in (*68*)

for solar cells would be straightforward applications due to the parametrisation property of the method. As mentioned in (*31*), problems with dielectric materials can surely be treated by the method as long as $dn_-/\lambda \leq 500$, or even more.

6. Summary

An overview of three of the most important integral equation methods for in-plane diffraction is given in Sect. 3 and their improvements as well as their pros and cons are highlighted, being the first overview since the comprehensive work in (*7, 28*). These are (1): the single equation integral method (IEM), (2): the modified integral method (MIM), and (3): the integral equation system method with parametrisation (IESMP), and the methods are discussed from a common perspective.

Then, in Sect. 4 an integral method for conical diffraction of a finitely conducting grating and a new method of a multilayer grating with separated interfaces of arbitrary finite conductivity are given in a common description. The recursive algorithm for the solution of the problems given in Sect. 4.3 and the determination of the scattering matrices given in Sect. 4.4 generalise the algorithm proposed by Maystre (*48*) for in-plane diffraction and are an extension of the method reported in (*36*). The numerical approximation of the scattering matrices is likewise an extension of (*36*).

The solution of the numerical systems is guaranteed under rather weak conditions: in the case of a single interface the system is solvable and provides a solution of the conical diffraction problem, if the ratios $\varepsilon_-/\varepsilon_+$ and μ_-/μ_+ of the permittivities and the permeabilities of both materials do not belong to an interval on the negative axis, which degenerates to the point -1 for a smooth grating profile. Similarly, for multilayer gratings with separated interfaces the presented algorithm solves off-plane diffraction, if on each interface the adjacent materials fulfil the above mentioned condition. Hence, one of the last real deficiencies of the integral method has been resolved for such gratings with inclusions.

The obtained results confirm that the code is accurate and efficient for solving off-plane diffraction problems from zero order gratings to arbitrary and real profiles of fabricated photonic and plasmonic structures, including surfaces with edges and gratings possessing a large period to wavelength ratio.

References

(1) Hutley, M.C. Diffraction Gratings. Academic: London, 1982.
(2) Kleemann, B.H.; Güther, R. Metal gratings with dielectric coating of variable thickness within a period. *J. mod. Opt.* **1991**, *38*, 897–910.
(3) Loewen, E.G.; Popov, E. Diffraction Gratings and Applications. Marcel Dekker: New York, 1997.
(4) Wilson, S.J.; Hutley, M.C. The optical properties of 'moth eye' antireflection surfaces. *Opt. Acta* **1982**, *29*, 993–1009.
(5) Noponen, E.; Vasara, A.; Turunen, J.; Miller, J.M.; et al. Synthetic diffractive optics in the resonance domain. *J. Opt. Soc. Am. A* **1992**, *9*, 1206–1213.
(6) Petit, R. (Ed.), Electromagnetic Theory of Gratings. Springer: Berlin, 1980.
(7) Maystre, D. Rigorous vector theories of diffraction gratings. In *Progress in Optics XXI*; Wolf, E. Ed.; Elsevier: Amsterdam, 1984; pp 1–67.
(8) Vasara, A.; Noponen, E.; Turunen, J.; Miller, J.M.; et al. Rigorous diffraction analysis of Dammann gratings. *Opt. Commun.* **1991**, *81*, 337–342.
(9) Noponen, E.; Turunen, J.; Vasara, A. Parametric optimization of multilevel diffractive optical elements by electromagnetic theory. *Appl. Opt.* **1992**, *31*, 5910–5912.
(10) Turunen, J.; Kuittinen, M.; Wyrowski, F. Diffractive Optics: Electromagnetic Approach. In *Progress in Optics XL*; Wolf, E. Ed.; Elsevier Science B. V.: Amsterdam, 2000; pp 343–388.
(11) Noponen, E.; Turunen, J.; Vasara, A. Electromagnetic theory and design of diffractive–lens arrays. *J. Opt. Soc. Am. A* **1993**, *10*, 434–443.
(12) Kleemann, B.H.; Güther, R. Zonal diffraction efficiencies and imaging of micro–Fresnel lenses. *J. mod. Opt.* **1998**, *45*, 1405–1420.
(13) Sheng, Y.; Feng, D.; Larochelle, S. Analysis and synthesis of circular diffractive lens with local linear grating model and rigorous coupled-wave theory. *J. Opt. Soc. Am. A* **1997**, *14*, 1562–1568.
(14) Shiono, T.; Kitagawa, M.; Setsune, K.; et al. Reflecting micro-Fresnel lenses and their use in an integrated focus sensor. *Appl. Opt.* **1989**, *28*, 3434–3442.

(15) Prather, D.W.; Mirotznik, M.S.; Mait, J.N. Boundary Element Method for Vector Modeling Diffractive Optical Elements. In: *Holographic and Diffractive Optics Technology II*, Proc. SPIE Vol. 2404; pp 28–39.
(16) Mirotznik, M.S.; Prather, D.W.; Mait, J.N. Hybrid Finite Element – Boundary Element Method for Vector Modeling Diffractive Optical Elements. In: *Holographic and Diffractive Optics Technology III*, Proc. SPIE Vol. 2689; pp 2–13.
(17) Prather, D.W.; Mirotznik, M.S.; Mait, J.N. Design of Subwavelength Diffractive Optical Elements Using a Hybrid Finite Element – Boundary Element Method. In: *Holographic and Diffractive Optics Technology III*, Proc. SPIE Vol. 2689; pp 14–23.
(18) Prather, D.W.; Mirotznik, M.S.; Mait, J.N. Boundary Integral Methods Applied to the Analysis of Diffractive Optical Elements. *J. Opt. Soc. Am. A* **1997**, *14*, 34–43.
(19) Schmitz, M.; Bryngdahl, O. Rigorous concept for the design of diffractive microlenses with high numerical aperture. *J. Opt. Soc. Am. A* **1997**, *14*, 901–906.
(20) Kleemann, B.H.; Ruoff, J.; Seeßelberg, M.; Kaltenbach, J.M.; Dobschal, H.J.; et al. Optical systems design with integrated rigorous vector diffraction. In: *Optical Design and Engineering II*, Mazuray, L., Wartmann, R. Eds.; , Proc. SPIE Vol. 5962; p. 596205.
(21) Herzig, H.P. (Ed.), Micro-Optics: Elements, Systems and Applications. Taylor & Francis: London, 1997.
(22) Turunen, J.; Wyrowski, F. (Eds.), Diffractive optics for industrial and commercial applications. Akademie: Berlin, 1997.
(23) Li, L.; Chandezon, J.; Granet, G.; et al. Rigorous and efficient grating-analysis method made easy for optical engineers. *Appl. Opt.* **1999**, *38*, 304–313.
(24) Loewen, E.G.; Maystre, D.; Popov, E.; et al. Echelles: scalar, electromagnetic and real-groove properties. *Appl. Opt.* **1995**, *34*, 1707–1727.
(25) Loewen, E.G.; Maystre, D.; Popov, E.; et al. Diffraction efficiency of echelles working in extremely high orders. *Appl. Opt.* **1996**, *35*, 1700–1704.
(26) Goray, L.I. The modified integral method and real electromagnetic properties of echelles. In: *Diffractive and Holographic Technologies for Integrated Photonic Systems*, Sutherland, R.I., Prather, D.W., Cindrich, I. Eds.; , Proc. SPIE Vol. 4291; pp 13–24.
(27) Kleemann, B.H.; Erxmeyer, J. Independent electromagnetic optimization of the two coating thicknesses of a dielectric layer on the facets of an echelle grating in Littrow mount. *J. mod. Opt.* **2004**, *51* (14), 2093–2110.
(28) Maystre, D. Integral Methods. In *Electromagnetic Theory of Gratings*; Petit, R. Ed.; Springer: Berlin, 1980; pp 63–100.
(29) Pomp, A. The integral method for coated gratings: computational cost. *J. mod. Opt.* **1991**, *38*, 109–120.
(30) Kleemann, B.H.; Mitreiter, A.; Wyrowski, F. Integral equation method with parametrization of grating profile – Theory and experiments. *J. mod. Opt.* **1996**, *43*, 1323–1349.
(31) Kleemann, B.H. Elektromagnetische Analyse von Oberflächengittern von IR bis XUV mittels einer parametrisierten Randintegralmethode: Theorie, Vergleich und Anwendungen. Ph.D. thesis, Technische Universität Ilmenau, Fachbereich Technische Optik 2002, Berlin: Mensch & Buch Verlag, 2003.
(32) Goray, L.I. Rigorous integral method in application to computing diffraction on relief gratings working in wavelength range from microwaves to X-ray. In: *Application and Theory of Periodic Structures*, Jannson, T. Ed.; , Proc. SPIE Vol. 2532; pp 427–433.
(33) Goray, L.I.; Seely, J.F. Efficiencies of Master, Replica, and Multilayer Gratings for the Soft-X-Ray-Extreme-Ultraviolet Range: Modeling Based on the Modified Integral Method and Comparisons with Measurements. *Appl. Opt.* **2002**, *41*, 1434–1445.
(34) Rathsfeld, A.; Schmidt, G.; Kleemann, B.H. On a fast integral equation method for diffraction gratings. *Comm. Comp. Phys.* **2006**, *1*, 984–1009.
(35) Schmidt, G. Boundary Integral Methods for Periodic Scattering Problems. In *Around the Research of Vladimir Maz'ya II. Partial Differential Equations*; International Mathematical SeriesVol. 12 Laptev, A. Ed.; Springer: New York, Dordrecht, Heidelberg, London, 2010; pp 337–364.
(36) Goray, L.I.; Schmidt, G. Solving conical diffraction grating problems with integral equations. *J. Opt. Soc. Am. A* **2010**, *27*, 585–597.
(37) Maystre, D. Sur la diffraction d'une onde plane par un réseau métallique de conductivité finie. *Opt. Commun.* **1972**, *6*, 50–54.
(38) Goray, L.I. Modified integral method for weak convergence problems of light scattering on relief grating. In: *Diffractive and Holographic Technologies for Integrated Photonic Systems*, Sutherland, R.I., Prather, D.W., Cindrich, I. Eds.; , Proc. SPIE Vol. 4291; pp 1–12.
(39) Maystre, D. Sur la diffraction d'une onde plane electromagnetique par un réseau métallique. *Opt. Commun.* **1973**, *8*, 216–219.
(40) Maystre, D. Sur la diffraction et l'absorption par les réseaux utilisés dans l'infraroige, le visible et l'ultraviolet. Ph.D. thesis, University of Aix-Marseille III, CNRS A.O. 9545, France, unpublished, 1974.
(41) Maystre, D. A new general integral theory for dielectric coated gratings. *J. Opt. Soc. Am.* **1978**, *68*, 490–495.
(42) Maystre, D. A new theory for multiprofile, buried gratings. *Opt. Commun.* **1978**, *26*, 127–132.
(43) Botten, L.C. A new formalism for transmission gratings. *Opt. Acta* **1978**, *25*, 481–499.
(44) Botten, L.C. Integral equation method for buried and bimetallic gratings. Ph.D. thesis, University of Tasmania, Hobart, 1978.
(45) Botten, L.C. A study of bi-metallic gratings. *J. Opt. (Paris)* **1980**, *11*, 161–166.
(46) Goray, L.I.; Seely, J.F.; Sadov, S.Y. Spectral separation of the efficiencies of the inside and outside orders of soft X-ray extreme-ultraviolet gratings at near normal incidence. *Journ. Appl. Physics* **2006**, *100*, 094901 1–13.
(47) Popov, E.; Bozhkov, B.; Maystre, D.; et al. Integral method for echelles covered with lossless or absorbing thin dielectric layers. *Appl. Opt.* **1999**, *38*, 47–55.
(48) Maystre, D. Electromagnetic study of photonic band gaps. *Pure Appl. Opt.* **1994**, *3*, 975–993.
(49) Maystre, D. Photonic crystal diffraction gratings. *Optics Express* **2001**, *8*, 209–216.
(50) Niethammer, W. Numerical application of Euler's transformation and its generalisations. *Num. Math.* **1980**, *34*, 271–283.
(51) Seely, J.F.; Goray, L.I. Normal Incidence Multilayer Gratings for the Extreme Ultraviolet Region: Experimental Measurements and Computational Modeling. In: *X-Ray Optics, Instruments, and Missions II*, Hoover, R.B., Walker, A.B. Eds.; , Proc. SPIE Vol. 3766; pp 364–370.
(52) Popov, E.; Nevière, M.; Gralak, B.; et al. The classical differential method, the rigorous coupled wave theory, and the

modal method: comparative analysis of convergence properties in staircase approximation. In: *Physics, Theory, and Applications of Periodic Structures in Optics*, Lalanne, P. Ed.; , Proc. SPIE Vol. 4438; pp 12–18.

(53) Goray, L.I.; Sadov, S.Y. Numerical modelling of coated gratings in sensitive cases. In: *Trends in Optics and Photonics*, Proc. OSA Vol. 75; pp 365–379.

(54) Pomp, A.; Kleemann, B.; Creutziger, J. *Beschreibung des Programmpaketes DACOTA*; , 1986. Interner Bericht, Karl–Weierstrass–Institut Berlin/Carl Zeiss Jena.

(55) Saad, Y.; Schultz, M.H. GMRES: A generalized minimal residual algorithm for solving nonsymmetric linear systems. *SIAM J. Sci. Stat. Comput.* **1986**, *7* (3), 856–869.

(56) Güther, R.; Korn, G.; Polze, S.; Schäfer, L.; Tesch, L.; et al. Herstellung und Untersuchung von holographischen Gittern für den infraroten Spektralbereich. *Opt. Commun.* **1984**, *50*, 291–295.

(57) Güther, R.; Kleemann, B.H.; Creutziger, J.; et al. Application of grating efficiency calculations. In: *Proceedings of Optika '88*, Lupkovics, G., Podmaniczky, A. Eds.; , Vol. 2; pp 610–613.

(58) Budzinski, C.; Güther, R.; Kleemann, B. Radiation-resistant gratings and their optical properties. *Optik* **1991**, *87*, 121–125.

(59) Kleemann, B.H.; Gatzke, J.; Jung, C.; et al. Design and efficiency characterization of diffraction gratings for applications in synchrotron monochromators by electromagnetic methods and its comparison with measurement. In: *Gratings and Grating Monochromators for Synchrotron Radiation*, Proc. SPIE Technical Conference Vol. 3150; pp 137–147.

(60) Linton, C.M. The Green's function for the two-dimensional Helmholtz equation in periodic domains. *J. Eng. Math.* **1998**, *33*, 377–402.

(61) Yeung, M.S.; Barouch, E. Three-dimensional nonplanar lithography simulation using a periodic fast multipole method. In: *Optical Microlithography X*, Fuller, G.E. Ed.; , Proc. SPIE Vol. 3051; pp 509–521.

(62) Yeung, M.S.; Barouch, E. Three-dimensional mask transmission simulation using a single integral equation method. In: *Optical Microlithography XI*, van den Hove, L. Ed.; , Proc. SPIE Vol. 3334; pp 704–713.

(63) Rao, S.M.; Wilton, D.R.; Glisson, A.W. Electromagnetic scattering by surfaces of arbitrary shape. *IEEE Trans. Antennas Propagat.* **1982**, *AP–30*, 409–418.

(64) Wu, Y.; Lu, Y.Y. Analyzing diffraction gratings by a boundary integral equation Neumann-to-Dirichlet map method. *J. Opt. Soc. Am. A* **2009**, *26*, 2444–2451.

(65) Wu, Y.; Lu, Y.Y. Dirichlet-to-Neumann map method for analyzing periodic arrays of cylinders with oblique incident waves. *J. Opt. Soc. Am. B* **2009**, *26*, 1442–1449.

(66) Wang, C.M.; Chang, Y.C.; Tsai, D.P. Spatial filtering by using cascading plasmonic gratings. *Optics Express* **2009**, *17*, 6218–6223.

(67) Seesselberg, M.; Kleemann, B.H. DOEs for Color Correction in Broad Band Optical Systems: Validity and Limits of Efficiency Approximations. In: *OSA International Optical Design Conference (IODC), Optical System Design*, Proc. SPIE Vol. 7652; pp 7652–65.

(68) Fahr, S.; Rockstuhl, C.; Lederer, F. Engineering the randomness for enhanced absorption in solar cells. *Appl. Phys. Lett.* **2008**, *92*, 171114–1–171114–3.

Table

N	CPU time [s]
50	0.1
100	0.3
200	0.5
400	2.2
800	11.1
1600	67.3

Table 1. CPU time for one efficiency calculation for the plasmonic multilayer structures of two stacked plasmonic gratings presented in Sect. 5.2 on an Intel® Core™ 2 Duo P8400 Processor @ 2.26 GHz.

Figure captions

Figure 1:
Cross section of a simple grating of period d with incidence direction $\boldsymbol{k}$, incidence angle θ, and conical angle ϕ.

Figure 2:
Cross section of a multilayer grating with inclusions.

Figure 3:
Photonic crystal diffraction grating with circular dielectric rods in air. Grating period D, photonic crystal period d.

Figure 4:
Efficiency of -1^{st} order for s–polarisation incidence (corresponds to a polarisation angle $\delta^{\mathrm{in}} = 90°$) at a photonic crystal diffraction grating of Figure 3 with $d = 1, D = 2d, r_{\mathrm{PhC}} = 0.2, R_{\mathrm{g}} = 0.15, n = 3$. Dashed line: in-plane Littrow mount, dotted line: conical incidence with $\phi = 10°$, $\theta = \theta_{\mathrm{L}}$, solid line: zero order reflection of a pure photonic crystal without grating and $\theta = \theta_{\mathrm{L}}$.

Figure 5:
Same as in Figure 4 but dotted curve for conical incidence with $\phi = 10°$, $\theta = \theta_{\mathrm{L}}$ and polarisation angle $\delta^{\mathrm{in}} = 80°$.

Figure 6:
Plasmonic multilayer structure consisting of two stacked plasmonic gratings of equal period $d = 500\,\mathrm{nm}$ and thickness $t = 50\,\mathrm{nm}$ with separation distance $w = 10\,\mathrm{nm}$. The elliptical silver rods are horizontally separated by air gaps of widths $S_1 = 150\,\mathrm{nm}$ and $S_2 = 50\,\mathrm{nm}$.

Figure 7:
In-plane TM polarisation angle dependent reflection of two stacked plasmonic gratings for $\lambda = 785\,\mathrm{nm}$. Solid curve: stacked rectangular silver rods presented in (*66*). Dashed curve: stacked elliptical silver rods.

Figure 8:
Same as in Figure 7 but for conical incidence with $\phi = 30°$ for two different polarisations. Solid and dotted curves belong to stacked rectangular silver rods. The two dashed curves belong to stacked elliptical silver rods. Dotted and long dashes are for polarisation angle $\delta^{\mathrm{in}} = 90°$ and solid and small dashes are for polarisation angle $\delta^{\mathrm{in}} = 52°$.

Figure 9:
Conical efficiency convergence for the investigated silver structures of Figure 6 presented in Sect. 5.2. Solid curve: elliptical rods, dashed curve: rectangular rods.

Figure 10:
Diffraction efficiency $\eta_1(\phi)$ of 1^{st} order transmission as function of conical angle ϕ in air at three wavelengths. In-plane angle: $\theta = 0°$, material of blaze grating: PMMA. Figure compares scalar analytical diffraction efficiency expression (4) of (*67*) with electromagnetic simulations for grating periods $d = 80\,\mu\mathrm{m}$ and $d = 20\,\mu\mathrm{m}$, respectively. Curves with diamonds (crosses, unmarked) correspond to wavelengths $\lambda_0 = 550\,\mathrm{nm}$ ($\lambda = 650\,\mathrm{nm}$, $\lambda = 450\,\mathrm{nm}$). Solid (dashed, dotted) curves correspond to scalar values (electromagnetic $d = 80\,\mu\mathrm{m}$, electromagnetic $d = 20\,\mu\mathrm{m}$).

Figures

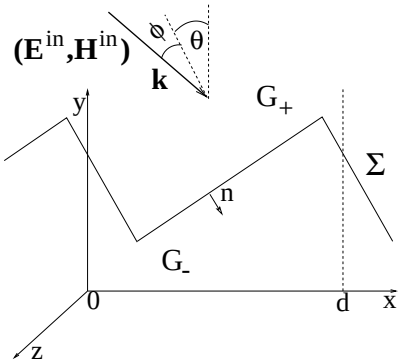

Figure 1. Cross section of a simple grating of period d with incidence direction $\boldsymbol{k}$, incidence angle θ, and conical angle ϕ.

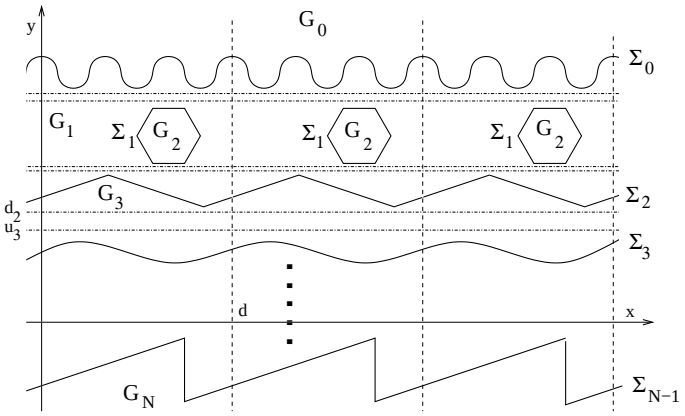

Figure 2. Cross section of a multilayer grating with inclusions

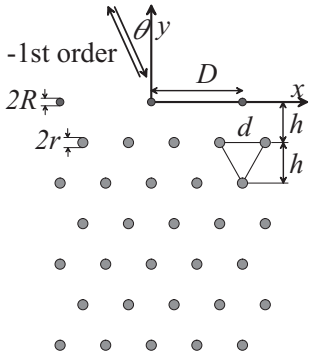

Figure 3. Photonic crystal diffraction grating with circular dielectric rods in air. Grating period D, photonic crystal period d.

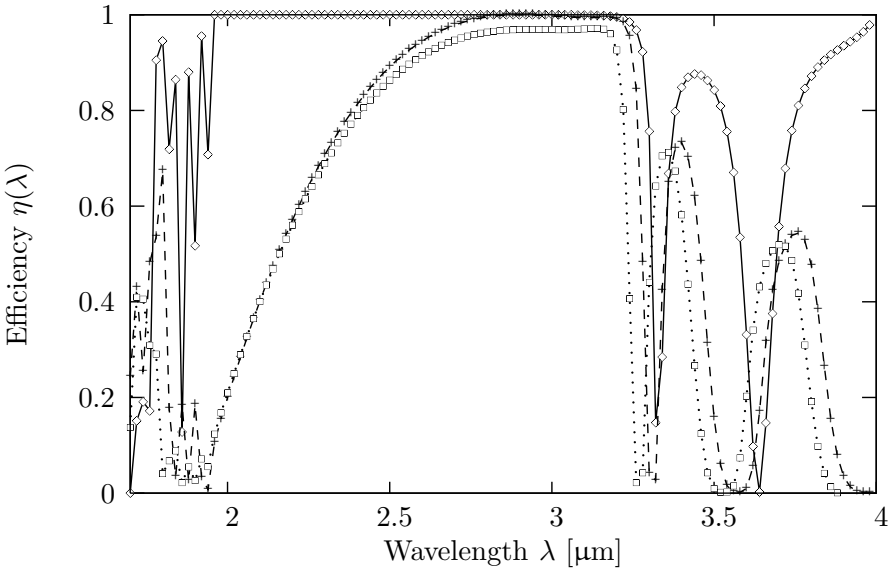

Figure 4. Efficiency of -1^{st} order for s–polarisation incidence (corresponds to a polarisation angle $\delta^{\text{in}} = 90°$) at a photonic crystal diffraction grating of Figure 3 with $d = 1, D = 2d, r_{\text{PhC}} = 0.2, R_{\text{g}} = 0.15, n = 3$. Dashed line: in-plane Littrow mount, dotted line: conical incidence with $\phi = 10°$, $\theta = \theta_{\text{L}}$, solid line: zero order reflection of a pure photonic crystal without grating and $\theta = \theta_{\text{L}}$.

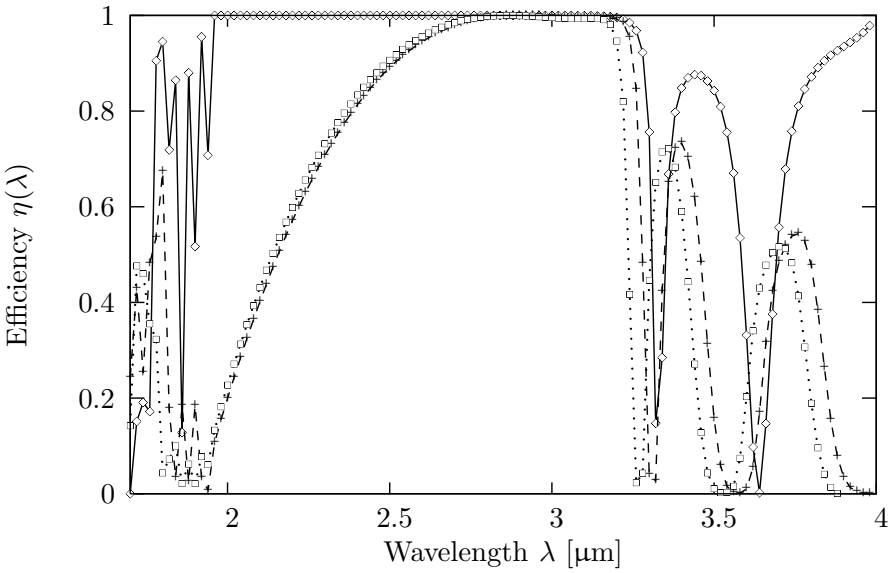

Figure 5. Same as in Figure 4 but dotted curve for conical incidence with $\phi = 10°$, $\theta = \theta_{\mathrm{L}}$ and polarisation angle $\delta^{\mathrm{in}} = 80°$.

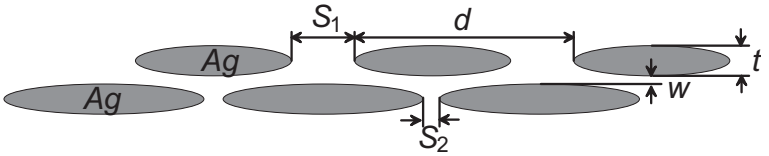

Figure 6. Plasmonic multilayer structure consisting of two stacked plasmonic gratings of equal period $d = 500\,\mathrm{nm}$ and thickness $t = 50\,\mathrm{nm}$ with separation distance $w = 10\,\mathrm{nm}$. The elliptical silver rods are horizontally separated by air gaps of widths $S_1 = 150\,\mathrm{nm}$ and $S_2 = 50\,\mathrm{nm}$.

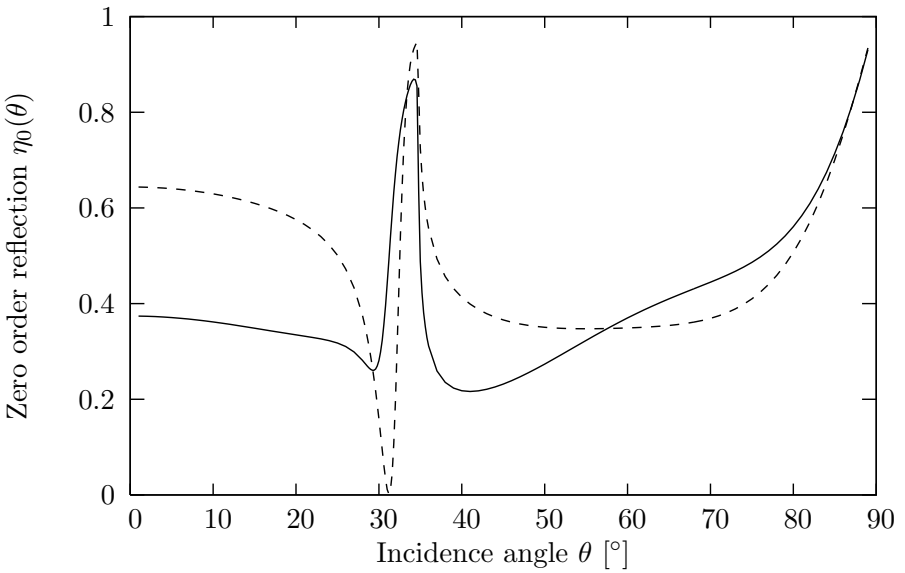

Figure 7. In-plane TM polarisation angle dependent reflection of two stacked plasmonic gratings for $\lambda = 785\,\mathrm{nm}$. Solid curve: stacked rectangular silver rods presented in (*66*). Dashed curve: stacked elliptical silver rods.

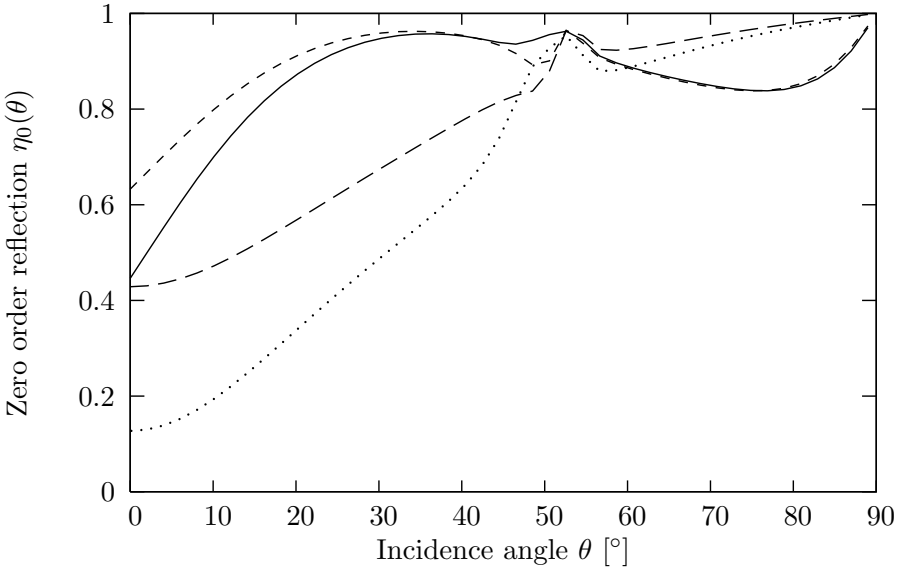

Figure 8. Same as in Figure 7 but for conical incidence with $\phi = 30°$ for two different polarisations. Solid and dotted curves belong to stacked rectangular silver rods. The two dashed curves belong to stacked elliptical silver rods. Dotted and long dashes are for polarisation angle $\delta^{\text{in}} = 90°$ and solid and small dashes are for polarisation angle $\delta^{\text{in}} = 52°$.

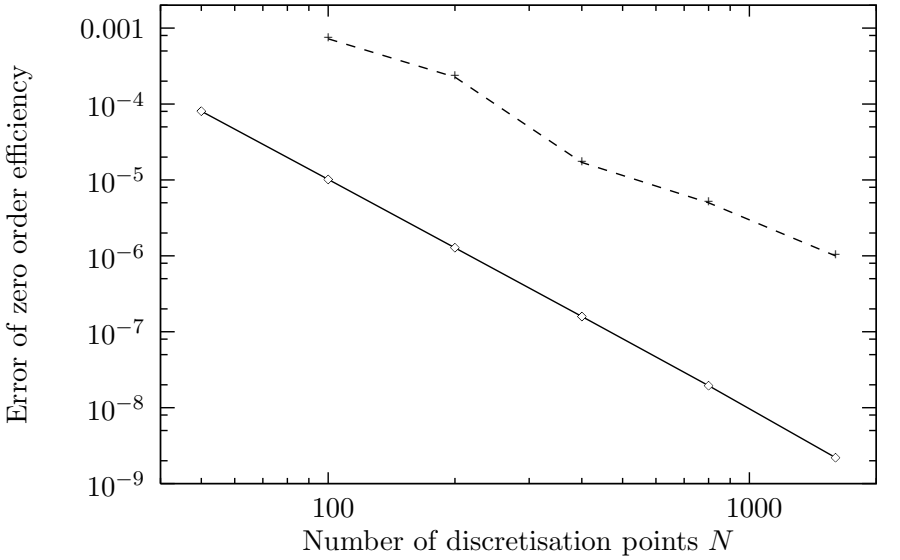

Figure 9. Conical efficiency convergence for the investigated silver structures of Figure 6 presented in Sect. 5.2. Solid curve: elliptical rods, dashed curve: rectangular rods.

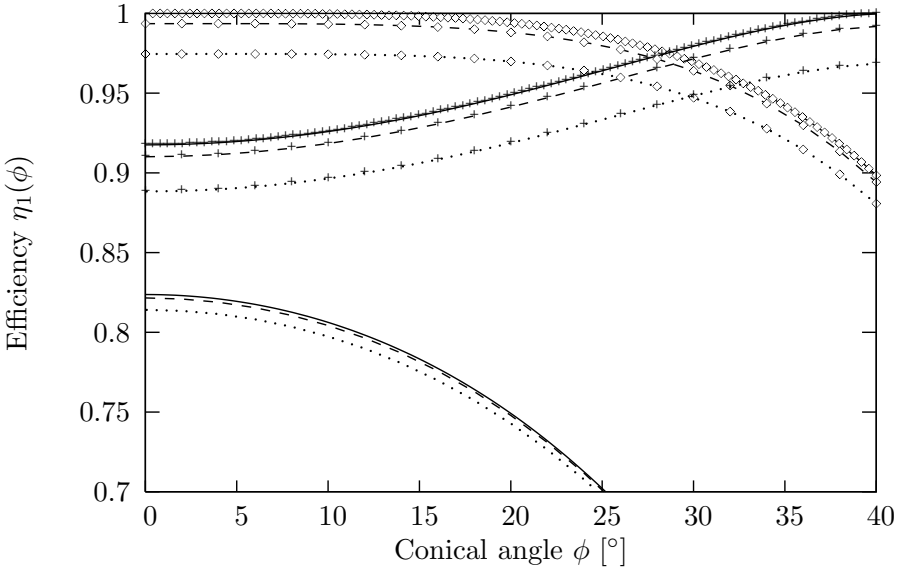

Figure 10. Diffraction efficiency $\eta_1(\phi)$ of 1$^{\text{st}}$ order transmission as function of conical angle ϕ in air at three wavelengths. In-plane angle: $\theta = 0°$, material of blaze grating: PMMA. Figure compares scalar analytical diffraction efficiency expression (4) of (*67*) with electromagnetic simulations for grating periods $d = 80\,\mu\text{m}$ and $d = 20\,\mu\text{m}$, respectively. Curves with diamonds (crosses, unmarked) correspond to wavelengths $\lambda_0 = 550\,\text{nm}$ ($\lambda = 650\,\text{nm}$, $\lambda = 450\,\text{nm}$). Solid (dashed, dotted) curves correspond to scalar values (electromagnetic $d = 80\,\mu\text{m}$, electromagnetic $d = 20\,\mu\text{m}$).